Article

Cell Metabolism

A_{2A} Receptor Activation Attenuates Hypertensive Cardiac Remodeling via Promoting Brown Adipose Tissue-Derived FGF21

Graphical Abstract

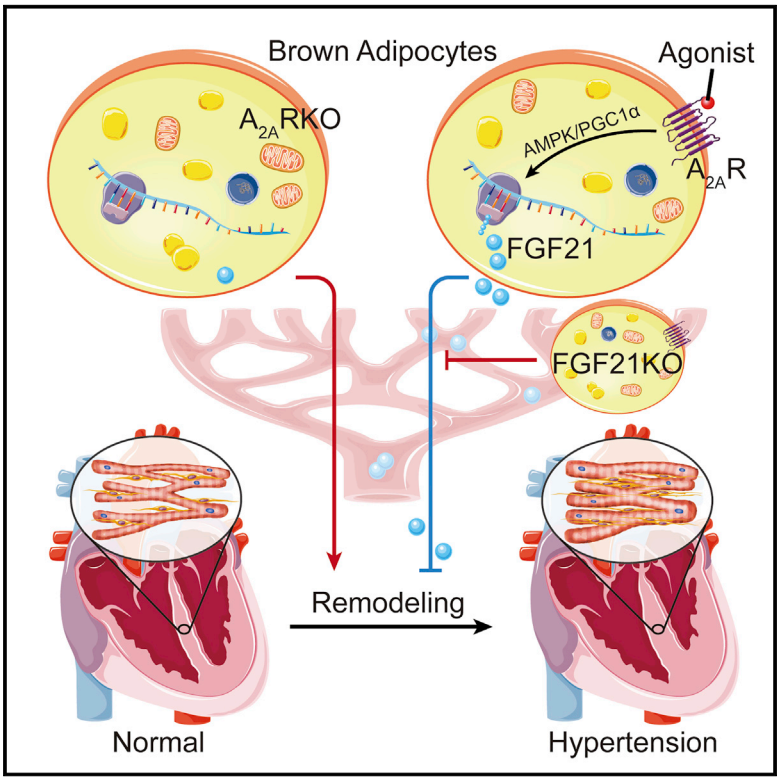

Authors

Cheng-Chao Ruan, Ling-Ran Kong, Xiao-Hui Chen, Yu Ma, Xiao-Xi Pan, Ze-Bei Zhang, Ping-Jin Gao

Correspondence

gaopingjin@sibs.ac.cn

In Brief

Ruan et al. uncover a direct crosstalk between brown adipose tissue (BAT) and the heart. Adenosine A_{2A} receptor ($A_{2A}R$) signaling in BAT mediates the release of the batokine, FGF21, which prevents hypertension-related cardiac damage.

Highlights

- Brown adipocyte is a direct target of $A_{2A}R$ in hypertension
- $A_{2A}R$ activation promotes FGF21 in brown adipocytes
- $A_{2A}R$/FGF21 axis provides a link between brown adipocyte and cardiac remodeling

Ruan et al., 2018, Cell Metabolism *28*, 1–14
October 2, 2018
https://doi.org/10.1016/j.cmet.2018.06.013

CellPress

Please cite this article in press as: Ruan et al., A_{2A} Receptor Activation Attenuates Hypertensive Cardiac Remodeling via Promoting Brown Adipose Tissue-Derived FGF21, Cell Metabolism (2018), https://doi.org/10.1016/j.cmet.2018.06.013

Cell Metabolism
Article

A_{2A} Receptor Activation Attenuates Hypertensive Cardiac Remodeling via Promoting Brown Adipose Tissue-Derived FGF21

Cheng-Chao Ruan,[1,2,3,4] Ling-Ran Kong,[1,2,4] Xiao-Hui Chen,[3] Yu Ma,[1] Xiao-Xi Pan,[1] Ze-Bei Zhang,[3] and Ping-Jin Gao[1,2,3,5,*]

[1]State Key Laboratory of Medical Genomics, Shanghai Key Laboratory of Hypertension, Ruijin Hospital, Shanghai Jiao Tong University School of Medicine, Shanghai, China

[2]Department of Hypertension, Shanghai Institute of Hypertension, Ruijin Hospital, Shanghai Jiao Tong University School of Medicine, Shanghai, China

[3]Key Laboratory of Stem Cell Biology, Shanghai Institutes for Biological Sciences, Chinese Academy of Sciences, Shanghai, China

[4]These authors contributed equally

[5]Lead Contact

*Correspondence: gaopingjin@sibs.ac.cn

https://doi.org/10.1016/j.cmet.2018.06.013

SUMMARY

Adipocytes play important roles in regulating cardiovascular health and disease. However, the molecular mechanism underlying the endocrine role of brown adipose tissue (BAT) in pathological cardiac remodeling remains unknown. Herein we show that adenosine A_{2A} receptor (A_{2A}R) knockout (A_{2A}RKO) causes interscapular BAT (iBAT) dysfunction, leading to accelerated cardiac remodeling in hypertension compared with wild-type (WT) mice. Surgical iBAT depletion induces dramatic cardiac remodeling in WT but not in A_{2A}RKO hypertensive mice. AMPK/PGC1α signaling-induced fibroblast growth factor 21 (FGF21) in brown adipocytes is required for A_{2A}R-mediated inhibition of hypertensive cardiac remodeling. Recombinant FGF21 administration improves cardiac remodeling in iBAT-depleted hypertensive mice. More importantly, brown adipocyte-specific A_{2A}RKO inhibits FGF21 production and accelerates cardiac damage in hypertension. Consistently, brown adipocyte-specific FGF21 knockout abolishes the effects of A_{2A}R agonism in attenuating hypertensive cardiac remodeling. Our findings reveal a distinctive endocrine role of BAT in hypertensive cardiac remodeling via activating A_{2A}R/FGF21 pathway.

INTRODUCTION

Hypertensive cardiac remodeling is characterized by left ventricular hypertrophy and interstitial fibrosis, which are the main causes of heart failure (Berk et al., 2007; Drazner, 2011). Recent studies show that adipocyte-derived adipokines are involved in the regulation of hypertensive heart disease (Mattu and Randeva, 2013; Mechanick et al., 2016). Hypertension is normally associated with increased sympathetic activity and release of catecholamines (Esler, 2015). These can activate brown adipose tissue (BAT) (Bahler et al., 2015; Hankir et al., 2016). In contrast to white adipose tissue (WAT), BAT dissipates energy though uncoupled respiration and thermogenesis, and protects against metabolic disorders (Kozak, 2010; Sidossis and Kajimura, 2015). Animal studies show that transgenic ablation of BAT is associated not only with obesity but also with systemic hypertension and cardiac fibrosis (Cittadini et al., 1999; Lowell et al., 1993). However, the precise mechanism underlying the interaction between BAT and cardiac remodeling is rarely investigated and remains elusive in hypertension.

Adenosine, an endogenous purine nucleoside, mediates a wide range of physiological and pathological functions through interacting with four cell surface receptor subtypes: A_1, A_{2A}, A_{2B}, and A_3 receptors (Borea et al., 2016). Among these, adenosine A_{2A} receptor (A_{2A}R), a Gs protein-coupled receptor, is abundantly expressed in various cell types and participates in the regulation of cardiovascular health and disease (Peleli and Carlstrom, 2017). A_{2A}R knockout (A_{2A}RKO) mice show aggressiveness, hypoalgesia, and high blood pressure phenotype (Ledent et al., 1997). Pharmacological activation of A_{2A}R attenuates hypertension-related cardiac remodeling (da Silva et al., 2017). However, A_{2A}R does not directly affect cardiac fibroblast function (Dubey et al., 1998). A recent report showed that pharmacological blockade or genetic deletion of A_{2A}R in mice causes a decrease in BAT-dependent thermogenesis, whereas treatment with A_{2A}R agonist significantly increases energy expenditure and protects against high-fat diet-induced obesity (Gnad et al., 2014). Therefore, we hypothesized that A_{2A}R protects against hypertensive cardiac remodeling via regulating BAT activity and related endocrine roles.

In the past two decades, a number of WAT-secreted adipokines have been identified after the initial discovery of leptin (MacDougald et al., 1995). These factors contribute directly to the regulation of chronic inflammation, vascular tone, and cardiovascular complications (Lau et al., 2017). However, the main adipokines released by WAT (e.g., leptin and adiponectin) are poorly expressed in BAT, especially when it is thermogenically

active (Villarroya et al., 2017). Recent studies have identified several BAT-derived endocrine factors (called batokines), including triiodothyronine (T3), neuregulin 4, fibroblast growth factor 21 (FGF21), and so on (Villarroya et al., 2017). Among these, FGF21, a member of the FGF superfamily, promotes glucose oxidation and protects against obesity and type 2 diabetes (Coskun et al., 2008; Gaich et al., 2013; Kliewer and Mangelsdorf, 2010). Under physiological conditions, the liver appears to be the main site for FGF21 production (Markan et al., 2014). However, thermogenic activation induces FGF21 gene expression in BAT and triggers the secretion of FGF21 from brown adipocytes (Lee et al., 2014). Besides the influence on energy metabolism, FGF21 has been shown to prevent cardiac hypertrophy, angiogenesis, atherosclerosis, and other cardiovascular disorders (Lin et al., 2015; Planavila et al., 2013; Yaqoob et al., 2014). However, whether A_{2A}R-mediated thermogenic activation of BAT promotes FGF21 production and whether BAT-derived FGF21 plays an endocrine role on cardiac remodeling in hypertension are still unknown.

In the present study, we examined the effect of A_{2A}RKO on the thermogenic activity and FGF21 expression in interscapular BAT (iBAT), as well as cardiac remodeling in deoxycorticosterone acetate (DOCA)-salt-induced hypertensive mice. We demonstrated that iBAT depletion reduced serum FGF21 level and induced dramatic cardiac remodeling in wild-type (WT) hypertensive mice, but these two effects were absent in A_{2A}RKO mice. Administration of recombinant human FGF21 dramatically improved cardiac remodeling in iBAT-depleted hypertensive mice. More importantly, we provided direct evidence to support the critical role of BAT A_{2A}R/FGF21 pathway in hypertensive cardiac remodeling by utilizing both brown adipocyte-specific A_{2A}R and FGF21 knockout mice. These findings demonstrate that A_{2A}R-mediated FGF21 release from BAT plays an endocrine protective role against hypertensive cardiac remodeling.

RESULTS

A_{2A}RKO Aggravates Hypertensive Cardiac Remodeling and Reduces BAT Activity

To determine the role of A_{2A}R in hypertensive cardiac remodeling, WT and A_{2A}RKO mice were utilized to induce DOCA-salt-sensitive hypertension and subjected to functional cardiac phenotyping measurement. A_{2A}RKO led to echocardiography-detectable dysfunction in DOCA-salt-treated mice, as demonstrated by decreases in ejection fraction (EF), fractional shortening (FS), and increases in diastolic left ventricular internal dimension (LVID; D) and interventricular septum (IVS; D) (Figures 1A and 1B). Next, Masson's trichrome (Masson), wheat germ agglutinin (WGA), and immunohistochemical (IHC) staining for collagen type I alpha 1 chain (Col1a1) and alpha smooth muscle actin (αSMA) were performed to analyze cardiac hypertrophy and interstitial fibrosis (Figures 1C and 1D). Histological analysis revealed that A_{2A}RKO increased cardiomyocyte size, fibrosis area, and expression of Col1a1 and αSMA compared with WT mice after DOCA-salt treatment (Figure 1E). A_{2A}RKO resulted in increased mRNA expression of hypertrophic markers, including atrial natriuretic polypeptide (*ANP*), brain natriuretic peptide (*BNP*), and myosin heavy chain beta (*βMHC*). Dramatic cardiac interstitial fibrosis in A_{2A}RKO mice was also evaluated by detecting elevated mRNA levels of fibrotic makers *Col1a1*, *αSMA*, and transforming growth factor β1 (*TGFβ*) (Figure 1F).

Next, we determined whether A_{2A}R directly regulated cardiac myocytes and fibroblasts functions *in vitro*. Treatment of neonatal mouse cardiac myocytes (NMCMs) and fibroblasts (CFs) with aldosterone showed significantly increased expression of *ANP*, *BNP*, and *βMHC*, or Col1a1, TGFβ, and αSMA. However, neither A_{2A}R agonist (CGS21680) nor antagonist (KW6002) affected the expression of these hypertrophic and fibrotic genes in NMCMs and CFs (Figures S1A and S1B). Neither agent had an effect on aldosterone-induced CF migration and proliferation (Figures S1C and S1D). These results suggest a likely indirect protective effect of A_{2A}R activation against hypertensive cardiac damage.

To identify potential target cells of A_{2A}R in hypertension, we detected A_{2A}R expression in different organs or tissues. Interestingly, A_{2A}R is abundant in adipose tissue compared with heart (Figure 2A). Especially, A_{2A}R expression was much higher in iBAT than other adipose tissues (Figure 2B). Moreover, hypertension induced A_{2A}R expression in iBAT, but not in heart (Figure 2C). Since A_{2A}R does not affect cardiac cell functions, we examined whether A_{2A}RKO-acceralated hypertensive cardiac remodeling is due to defect in iBAT thermogenesis. As expected, DOCA-salt treatment significantly promoted iBAT thermogenic activity including smaller-sized adipocyte and increased uncoupling protein 1 (UCP1) staining, but this effect was absent in A_{2A}RKO mice (Figures 2D and 2E). Consistently, hypertension only induced expression of thermogenic genes (*UCP1*, *PPARγ*, *PRDM16*, and *CIDEA*) in the iBAT of WT mice, but not in A_{2A}RKO mice (Figure 2F). In addition, we also detected thermogenic genes expression in subcutaneous WAT (sWAT) and visceral WAT (vWAT) of hypertensive mice. DOCA-salt treatment caused a slight increase of expression of thermogenic genes in sWAT of WT mice, but not in A_{2A}RKO mice (Figures S2A and S2B). However, these genes in the vWAT did not change after DOCA-salt treatment (Figures S2C and S2D). *In vitro* treatment with CGS21680 promoted, whereas KW6002 inhibited, brown adipogenesis and thermogenic gene expression in primary brown adipocytes (Figures 3A and 3B). More importantly, WT brown adipocyte-conditioned medium attenuated aldosterone-induced fibrotic marker expression in CFs, but this effect was absent in A_{2A}RKO brown adipocyte-conditioned medium (Figure 3C). These results clearly indicate a potential endocrine role of BAT on cardiac remodeling in hypertensive mice.

A_{2A}R Regulates FGF21 Expression in BAT

As an important metabolic regulator, FGF21 is known to improve metabolic health by preventing lipid accumulation in adipose tissues (Holland et al., 2013). Although FGF21 is poorly expressed in WAT, thermogenic activation induces FGF21 expression in brown adipocytes (Lee et al., 2014). Except for the autocrine role of FGF21 on adipose tissue, the endocrine role of FGF21 may connect altered BAT function to cardiac remodeling. Recent studies showed that FGF21 knockout accelerates pathological cardiac damage in different animal models (Planavila et al., 2015; Zhang et al., 2015). Therefore, we measured FGF21 expression in heart and iBAT and found that FGF21 expression in iBAT was almost 10-fold greater than that in heart in DOCA-salt hypertensive mice (Figure 3D). To determine whether

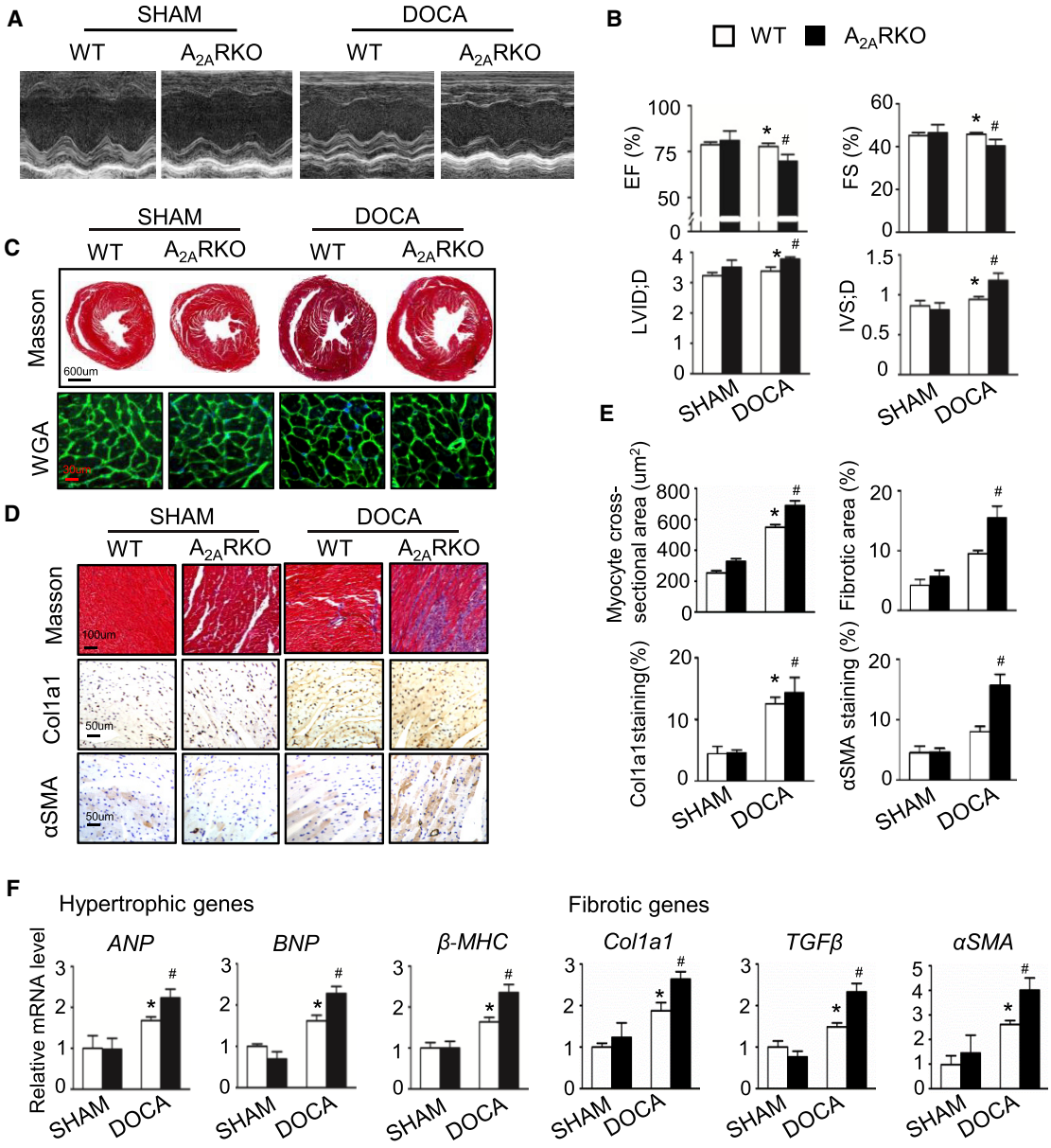

Figure 1. A_{2A}RKO Accelerates Cardiac Remodeling in Hypertensive Mice

(A) Representative echocardiography images of WT or A_{2A}RKO mice after SHAM or DOCA-salt treatment for 2 weeks.

(B) Quantitative analysis of ejection fraction (EF), fractional shortening (FS), left ventricular internal dimension (LVID; D), and interventricular septum (IVS; D) in diastolic phase obtained from echocardiography.

(C) Representative cross-sections of heart stained for Masson or WGA, in WT or A_{2A}RKO SHAM and DOCA-salt hypertensive mice.

(D) Representative cross-sections of heart stained for Masson, Col1a1, and αSMA in WT or A_{2A}RKO SHAM and DOCA-salt hypertensive mice.

(E) Quantitative analysis of cardiomyocyte size (WGA staining), fibrotic area (blue area in Masson staining), Col1a1, and αSMA signals.

(F) qPCR analysis of mRNA expression levels of hypertrophic and fibrotic genes in the heart.

Data are presented as means ± SEM; n = 6/group; *p < 0.05 versus SHAM WT group, #p < 0.05 versus DOCA WT group.

A_{2A}R-mediated BAT activation promotes FGF21 expression, we examined the effects of A_{2A}R agonist CGS21680 and A_{2A}R antagonist KW6002 on FGF21 expression *in vitro*. CGS21680 promoted, whereas KW6002 inhibited, FGF21 expression and release in brown adipocytes (Figures 3E and 3F). In contrast, the effect of A_{2A}R agonist or antagonist in altering FGF21 production was not observed in NMCMs and CFs (Figures S3A and S3B). Consistently, FGF21 expression in A_{2A}RKO brown adipocytes was much less than in WT adipocytes and adenosine-induced FGF21 expression was absent in A_{2A}RKO brown adipocytes (Figure 3G). More importantly, we found that recombinant FGF21 (rFGF21) attenuated aldosterone-induced hypertrophic gene expression in NMCMs (Figure S3C) and it inhibited fibrotic gene expression in CFs *in vitro* (Figure S3D). Since FGF21

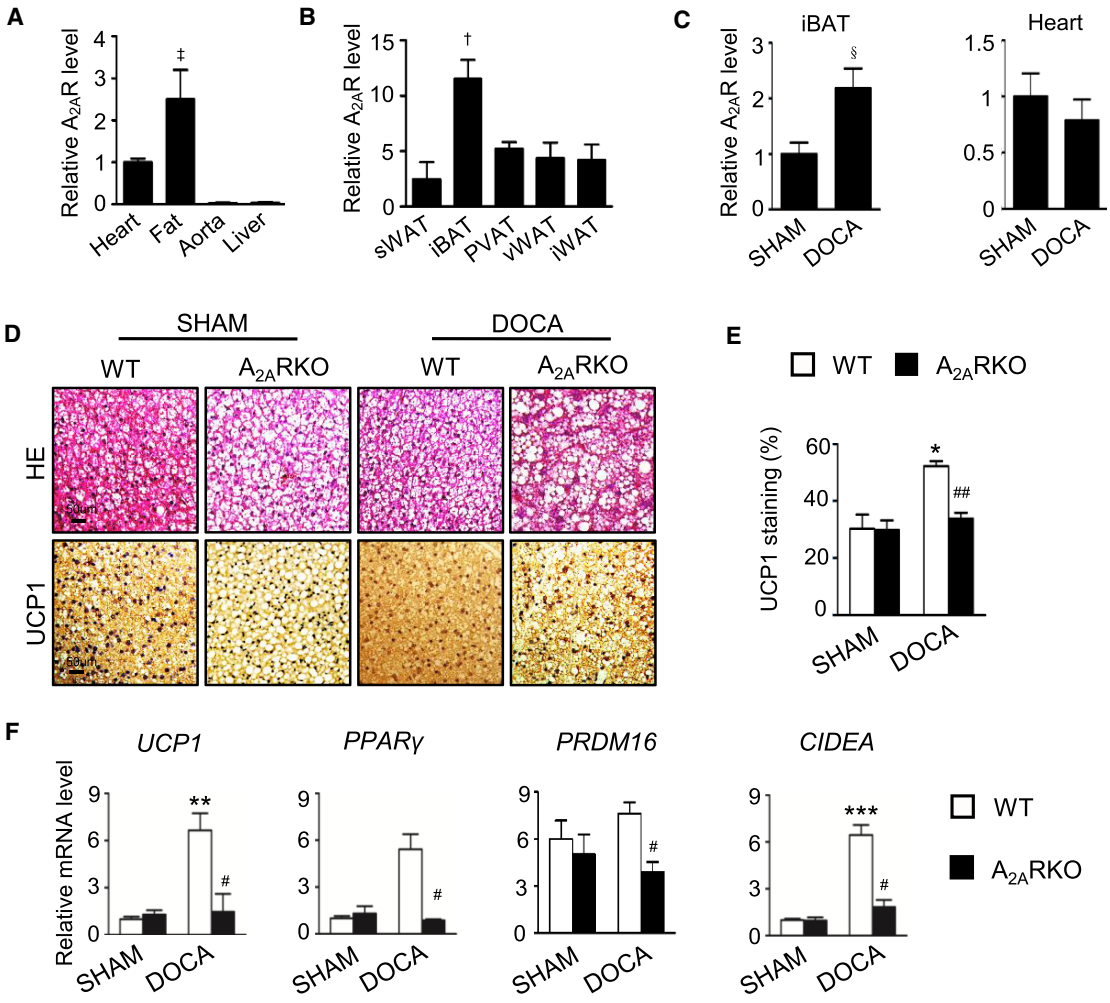

Figure 2. A_{2A}RKO Reduces iBAT Activity in Hypertensive Mice

(A) qPCR analysis of A_{2A}R mRNA expression levels in different tissues or organs ($^{‡}p < 0.05$ versus heart).

(B) qPCR analysis of A_{2A}R mRNA expression levels in different adipose tissues, sWAT indicates subcutaneous WAT, iBAT indicates interspacular BAT, PVAT indicates perivascular adipose tissue, vWAT indicates visceral WAT, iWAT indicates inguinal WAT ($^{†}p < 0.05$ versus sWAT).

(C) qPCR analysis of A_{2A}R mRNA expression levels in iBAT and heart from SHAM and DOCA-salt-treated mice ($^{§}p < 0.05$ versus SHAM).

(D) Representative H&E and UCP1 staining images of iBAT from WT or A_{2A}RKO mice after SHAM or DOCA-salt treatment for 2 weeks.

(E) Quantitative analysis of UCP1 signal in WT or A_{2A}RKO SHAM and DOCA-salt hypertensive mice.

(F) qPCR analysis of mRNA expression levels of thermogenic genes in the iBAT.

Data are presented as means ± SEM; n = 6/group; For (E) and (F), $^{*}p < 0.05$, $^{**}p < 0.01$, $^{***}p < 0.001$ versus SHAM WT group, $^{\#}p < 0.05$, $^{\#\#}p < 0.01$ versus DOCA WT group.

functions by preferentially signaling through a receptor complex composed of FGF receptors and co-receptor beta-klotho (KLB) (Chen et al., 2017), we detected FGF21 receptor expression in NMCMs and CFs, including *KLB*, *FGFR1*, *FGFR2*, *FGFR3*, and *FGFR4*. Among these, rFGF21 notably stimulated *KLB* and *FGFR1* expression, but not others (Figures S3E and S3F). Co-immunoprecipitation (coIP) assay further showed that FGF21 directly interacted with KLB and FGFR1 (Figure S3G). *In vivo*, A_{2A}RKO inhibited FGF21 expression in iBAT, but not in the heart and liver of hypertensive mice (Figure 3H). Besides, A_{2A}RKO resulted in decreased serum FGF21 level in hypertensive mice (Figure 3I). Collectively, these studies provide strong evidence suggesting that A_{2A}R-mediated iBAT theromgenic activation promotes FGF21 production and thus protects against hypertensive cardiac remodeling.

AMPK/PGC1α Signaling Is Involved in A_{2A}R-Mediated FGF21 Expression in BAT

We next determined the signaling pathway that regulated A_{2A}R-mediated FGF21 expression in brown adipocytes. Previous studies showed that AMPK, AKT, PKA, and MAPK are involved in the regulation of FGF21 expression (Alonge et al., 2017; Chau et al., 2010; Jeanson et al., 2016). Herein we showed that adenosine or A_{2A}R agonist CGS21680 quicklyy stimulated AMPK phosphorylation (Figures 4A and S4A) and subsequently promoted transcription factor coactivator PGC1α expression in

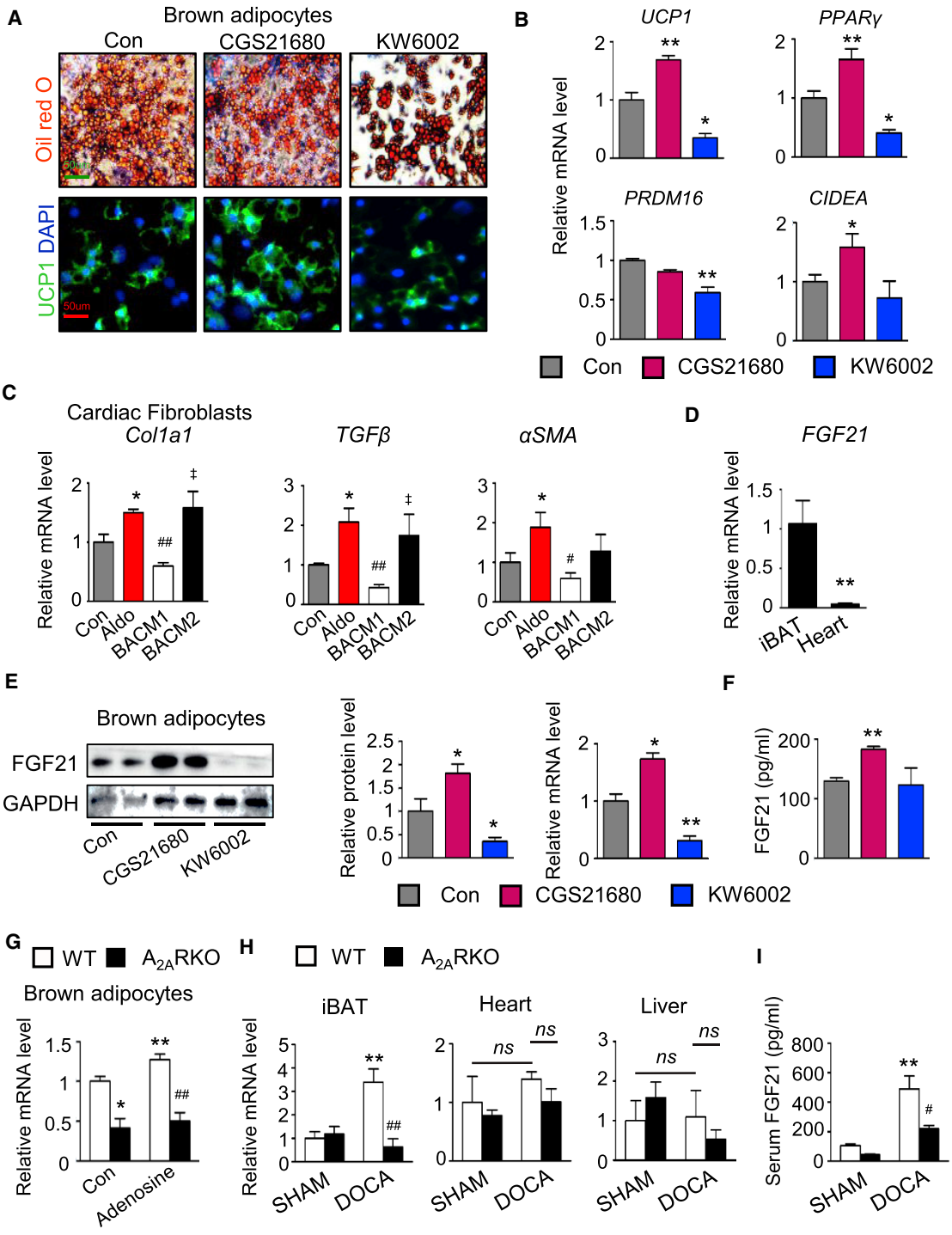

Figure 3. A_{2A}R Promotes FGF21 Expression in Brown Adipocytes

(A) Representative oil red O and UCP1 staining in CGS21680 (150 nM) or KW6002 (100 nM) treated primary brown adipocytes.

(B) qPCR analysis of thermogenic genes in brown adipocytes from WT mice with CGS21680 or KW6002 treatment (n = 6) (*p < 0.05, **p < 0.01 versus CON group).

(C) qPCR analysis of genes associated with fibrosis in cardiac fibroblasts after aldosterone (Aldo, 100 nM) stimulation with or without brown adipocyte-conditioned medium infusion. BACM1 indicates brown adipocyte-conditioned medium of WT mice. BACM2 indicates brown adipocyte-conditioned medium of A_{2A}RKO mice (n = 6) (*p < 0.05 versus CON group, #p < 0.05, ##p < 0.01 versus Aldo group, ‡p < 0.05 versus BACM1 group).

(D) Relative FGF21 mRNA level in iBAT and heart in adult WT mice (n = 5) (**p < 0.01 versus iBAT).

(E) Western blot and qPCR analysis of FGF21 level of primary brown adipocytes from WT mice with CGS21680 or KW6002 treatment (n = 6) (*p < 0.05, **p < 0.01 versus Con group).

(F) FGF21 level in primary brown adipocyte-conditioned medium with CGS21680 or KW6002 treatment (n = 6) (*p < 0.05, **p < 0.01 versus Con group).

(legend continued on next page)

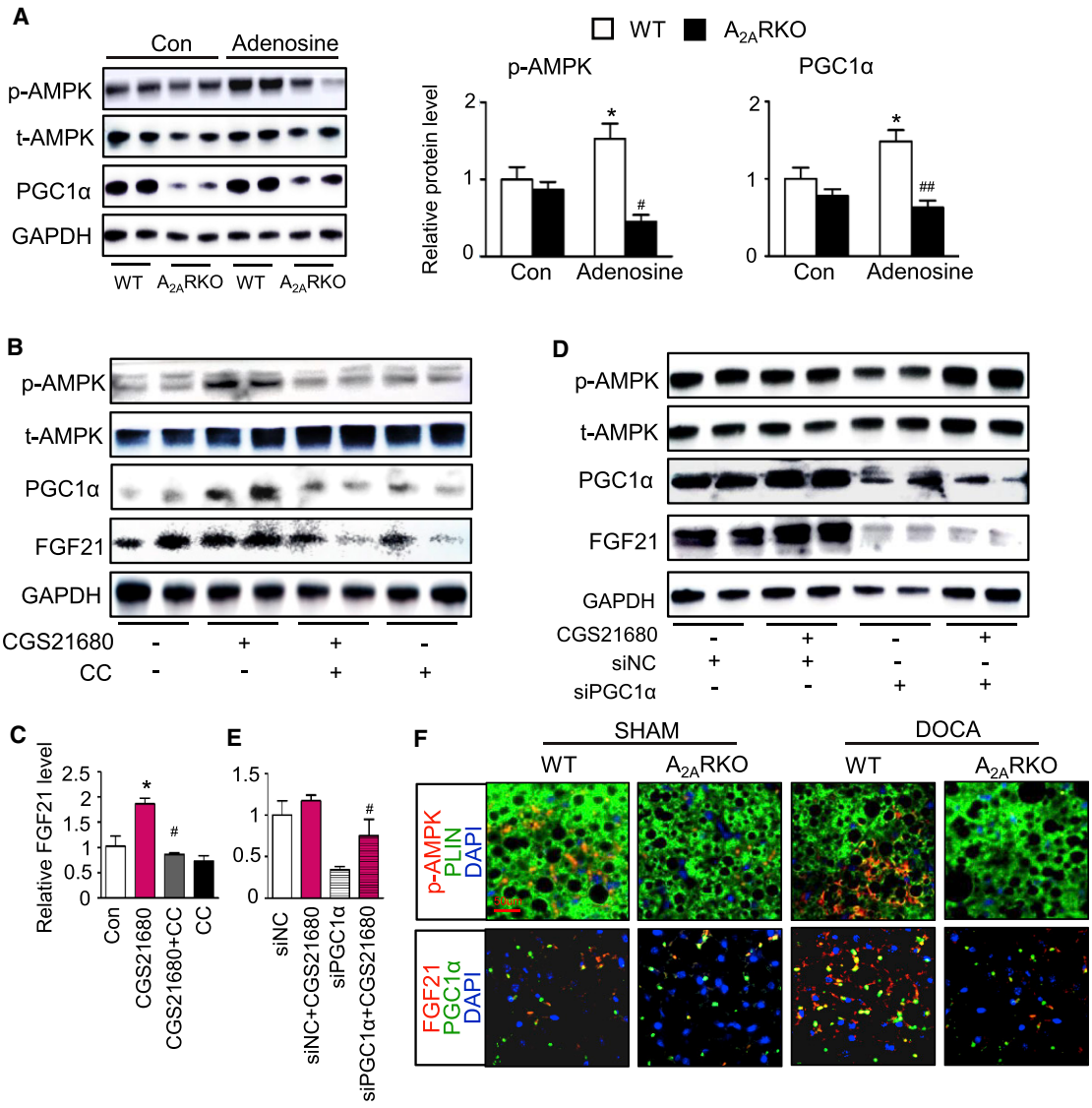

Figure 4. Blockade of AMPK/PGC1α Signaling Pathway Attenuates A_{2A}R-Mediated FGF21 Expression in Brown Adipocytes

(A) Western blot analysis of AMPK phosphorylation and PGC1α expression levels in WT or A_{2A}RKO adipocytes treated with adenosine (100 nm). Quantitative results are shown on the right (n = 6) (*p < 0.05 versus Con WT group, #p < 0.05, ##p < 0.01 versus WT adenosine group).

(B and C) Western blot analysis of p-AMPK, PGC1α, and FGF21 expression in primary adipocytes treated with AMPK inhibitor compound C (CC, 20 μm). Quantitative analysis of FGF21 is shown in the lower panel (n = 6) (*p < 0.05 versus Con group, #p < 0.05 versus CGS21680 group).

(D and E) Western blot analysis of p-AMPK, PGC1α, and FGF21 expression in primary adipocytes transfected with PGC1α shRNA lentivirus. Quantitative analysis of FGF21 is shown in the lower panel (n = 6) (#p < 0.05 versus siNC + CGS21680 group).

(F) Representative p-AMPK, PGC1α, and FGF21 immunostaining of iBAT in WT or A_{2A}RKO SHAM and DOCA-salt hypertensive mice.

Data are presented as means ± SEM.

brown adipocytes, whereas these effects were absent in A_{2A}RKO mouse brown adipocytes (Figure 4A). In contrast, PKA, AKT, and P38 MAPK phosphorylation did not change after CGS21680 treatment in brown adipocytes (Figure S4A). To determine whether AMPK/PGC1αis necessary for A_{2A}R-mediated FGF21 expression, we first utilized AMPK inhibitor

(G) qPCR analysis of FGF21 level of primary brown adipocyte from WT and A_{2A}RKO mice with or without adenosine (100 nM) treatment (n = 6) (*p < 0.05, **p < 0.01 versus WT Con group, ##p < 0.01 versus WT adenosine group).

(H) Relative FGF21 mRNA level in iBAT, heart and liver of WT and A_{2A}RKO mice after SHAM or DOCA-salt treatment for 2 weeks (n = 6) (**p < 0.01 versus SHAM WT group, ##p < 0.01 versus DOCA WT group, ns indicates no statistical difference).

(I) Relative FGF21 level in serum of WT and A_{2A}RKO mice after SHAM or DOCA-salt treatment for 2 weeks (n = 6) (**p < 0.01 versus SHAM WT group, #p < 0.05 versus DOCA WT group).

Data are presented as means ± SEM.

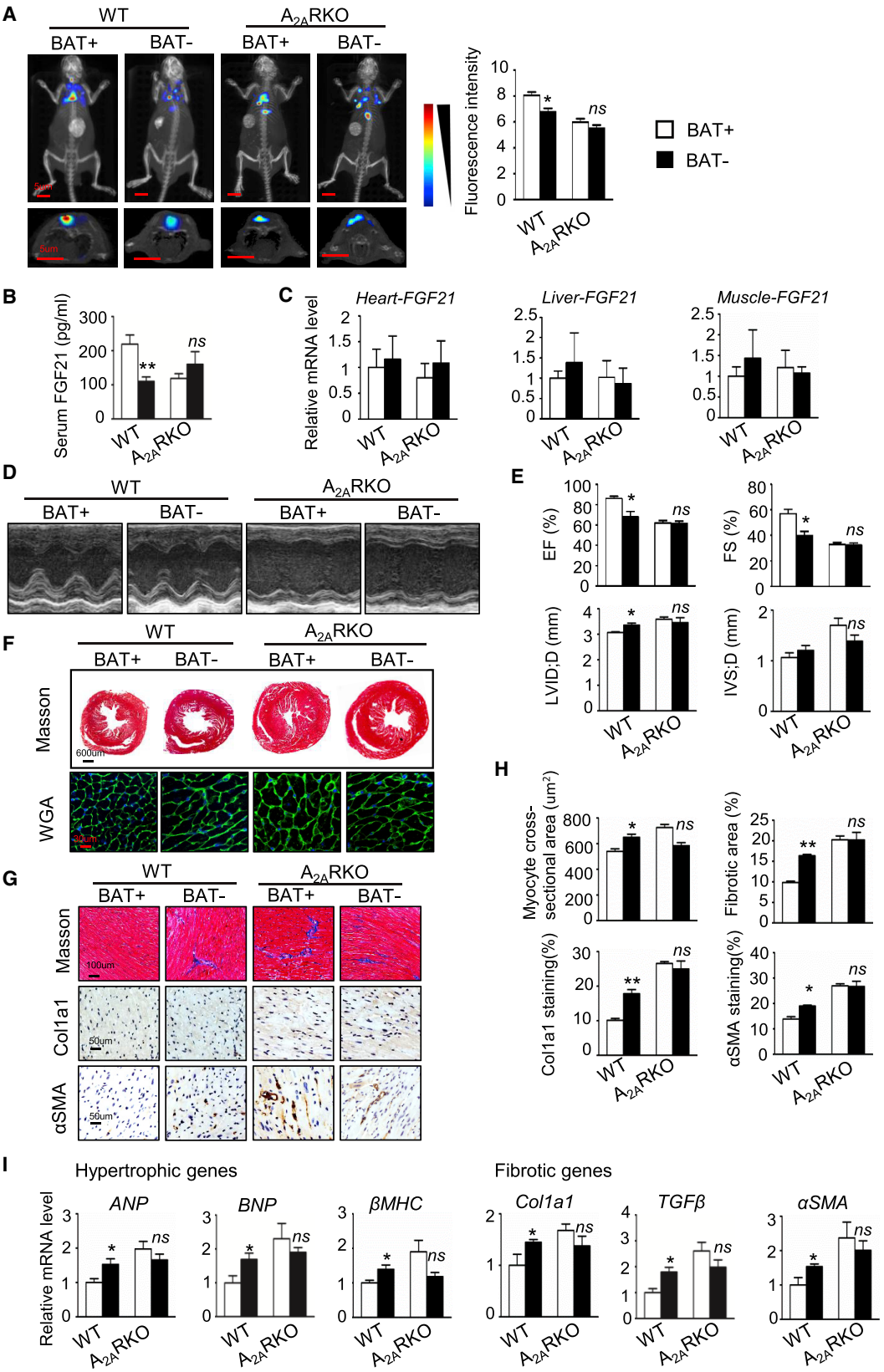

(legend on next page)

compound C (CC) to pretreat adipocytes. CC not only inhibited CGS21680-induced AMPK phosphorylation and PGC1α upregulation, but also reversed CGS21680-induced FGF21 expression (Figures 4B and 4C). To rule out a possible role of PGC1α in regulating FGF21 expression, lentivirus PGC1α small hairpin RNA (shRNA) was used to knock down PGC1α expression in adipocytes (Figures S4B and S4C). PGC1α shRNA attenuated CGS21680-induced FGF21 expression without changing AMPK phosphorylation (Figures 4D and 4E). In addition, we also measured AMPK phosphorylation and PGC1α expression in WT and A_{2A}RKO hypertensive mice. DOCA-salt treatment resulted in an increased AMPK phosphorylation and PGC1α upregulation accompanied by enhanced FGF21 staining in iBAT, but these effects were absent in A_{2A}RKO hypertensive mice (Figure 4F). In sWAT and vWAT, no changes in AMPK phosphorylation, or PGC1α and FGF21 expression, was detected in both WT and A_{2A}RKO hypertensive mice (Figure S4D). These data suggest that A_{2A}R-mediated FGF21 expression is most likely mediated through promoting AMPK phosphorylation and upregulation of downstream PGC1α in brown adipocytes.

Bat-Derived Fgf21 Protects against Hypertensive Cardiac Remodeling

To determine whether BAT is necessary for A_{2A}R activation in regulating cardiac remodeling, we surgically removed iBAT in WT and A_{2A}RKO hypertensive mice. After 14 days, BAT activity was estimated by a deep-red fluorescent micellar probe, SRFluor680, which has been showed to be accumulated in iBAT regardless of mouse species (Rice et al., 2015). Fluorescence imaging combined with microCT showed a dramatic decreased fluorescent density in the interscapular region after iBAT depletion (BAT−) in WT mice compared with sham operated mice (BAT+) (Figure 5A). Serum FGF21 level was decreased after iBAT depletion in WT mice, but not in A_{2A}RKO mice (Figure 5B). In contrast, heart, liver, and muscle FGF21 mRNA expression did not change after iBAT depletion in WT or A_{2A}RKO mice (Figure 5C). More importantly, iBAT depletion augmented DOCA-salt-induced cardiac dysfunction and remodeling in WT mice, as reflected by decreased EF and FS, and increased LVID and IVS (Figures 5D and 5E). Masson, WGA, and IHC staining results also showed that iBAT depletion increased cardiomyocyte size, and Col1a1 and αSMA expression in WT mice (Figures 5F–5H). Consistently, qPCR assay showed that these pathological changes were accompanied by upregulation of hypertrophic and fibrotic genes, including *ANP*, *BNP*, *βMHC*, *Col1a1*, *TGFβ*, and *αSMA* (Figure 5I). However, hypertensive cardiac remodeling did not show further aggravation after iBAT depletion in A_{2A}RKO mice (Figures 5D–5I). These findings implicate that BAT participates in the effect of A_{2A}R activation on cardiac function.

To determine the direct protective effects of FGF21 on cardiac remodeling, we administered rFGF21 for 2 weeks by daily intraperitoneal injection to DOCA-salt mice with or without iBAT depletion. Treatment with rFGF21 had no effect on hypertensive cardiac remodeling when iBAT was intact (BAT+). By contrast, in iBAT-depleted mice, in which FGF21 level is decreased, treatment with rFGF21 ameliorated cardiac damage in DOCA-salt-induced hypertension (Figures S5A–S5F). The coIP results showed that rFGF21 protein directly interacted with KLB and FGFR1 in the heart (Figure S5G). These data suggest that A_{2A}R-mediated FGF21 production in iBAT protects against hypertensive cardiac remodeling.

Brown Adipocyte-Specific A_{2A}RKO Accelerates Hypertensive Cardiac Remodeling

To provide more direct evidence that BAT is required for A_{2A}R-mediated inhibition of hypertensive cardiac remodeling, we generated both brown adipocyte-specific A_{2A}RKO (BAAKO) and cardiac fibroblast-specific A_{2A}RKO (CFAKO) mice. $A_{2A}R^{flox/+}$ mice were bred with UCP1-Cre (for brown adipocyte KO) or SM22α-Cre (for cardiac fibroblast KO) mice, the UCP1-Cre+;$A_{2A}R^{flox/flox}$ (BAAKO) and littermates UCP1-Cre-;$A_{2A}R^{flox/flox}$ (Con-BA) mice, or SM22α-Cre+;$A_{2A}R^{flox/flox}$ (CFAKO) and littermates SM22α-Cre-;$A_{2A}R^{flox/flox}$ (Con-CF) mice were treated with DOCA-salt to induce hypertension (Figures 6A and S6A). As UCP1 is essential for uncoupling respiration and dissipating chemical energy as heat in brown adipocytes, BAAKO resulted in absolutely knockout of A_{2A}R expression in BAT, but not in other tissues (Figure 6B). Likewise, CFAKO resulted in knockout of A_{2A}R in heart, whereas it did not affect A_{2A}R expression in other tissues (Figure S6B), indicating the success of generation of brown adipocyte-specific or cardiac fibroblast-specific deletion of A_{2A}RKO mice. BAAKO resulted in accelerated cardiac remodeling, including echocardiogram dysfunction, increased left ventricular hypertrophy and enhanced interstitial fibrosis compared with Con-BA mice after DOCA-salt treatment (Figures 6C–6I). In contrast, CFAKO had no effect on cardiac remodeling in hypertension compared with Con-CF mice (Figures S6C–S6I). FGF21 expression was blocked in iBAT and serum FGF21 level was reduced in BAAKO hypertensive mice (Figure 6J), whereas BAAKO did not affect FGF21 expression in heart, liver, and muscle (Figure 6K). Consistently, BAAKO

Figure 5. IBAT Depletion Accelerates Hypertensive Cardiac Remodeling in WT but Not in A_{2A}RKO Mice

(A) Representative fluorescence imaging combined with microCT of SHAM (BAT+) and iBAT-depleted (BAT−) WT or A_{2A}RKO mice after intravenous injection of SRFluor680 for 6 hr. Quantitative results are shown on the right.

(B) ELISA analysis of serum FGF21 levels in WT and A_{2A}RKO mice with or without iBAT.

(C) FGF21 mRNA expression levels in heart, liver, and muscle of WT and A_{2A}RKO mice with or without iBAT.

(D) Representative echocardiography images form WT and A_{2A}RKO mice with or without iBAT.

(E) Quantitative analysis of EF, FS, LVID; D, and IVS; D obtained from echocardiography.

(F) Representative cross-sections of heart stained for Masson and WGA in WT and A_{2A}RKO mice with or without iBAT.

(G) Representative cross-sections of heart stained for Masson, Col1a1, and αSMA in WT and A_{2A}RKO mice with or without iBAT.

(H) Quantitative analysis of cardiomyocyte size (WGA staining), fibrotic area (blue area in Masson staining), Col1a1, and αSMA signals.

(I) qPCR analysis of mRNA expression levels of hypertrophic and fibrotic genes in the heart.

Data are presented as means ± SEM; n = 6–10/group; *p < 0.05, **p < 0.01 versus WT BAT + hypertensive mice, ns indicates no statistical difference versus A_{2A}RKO BAT + hypertensive mice.

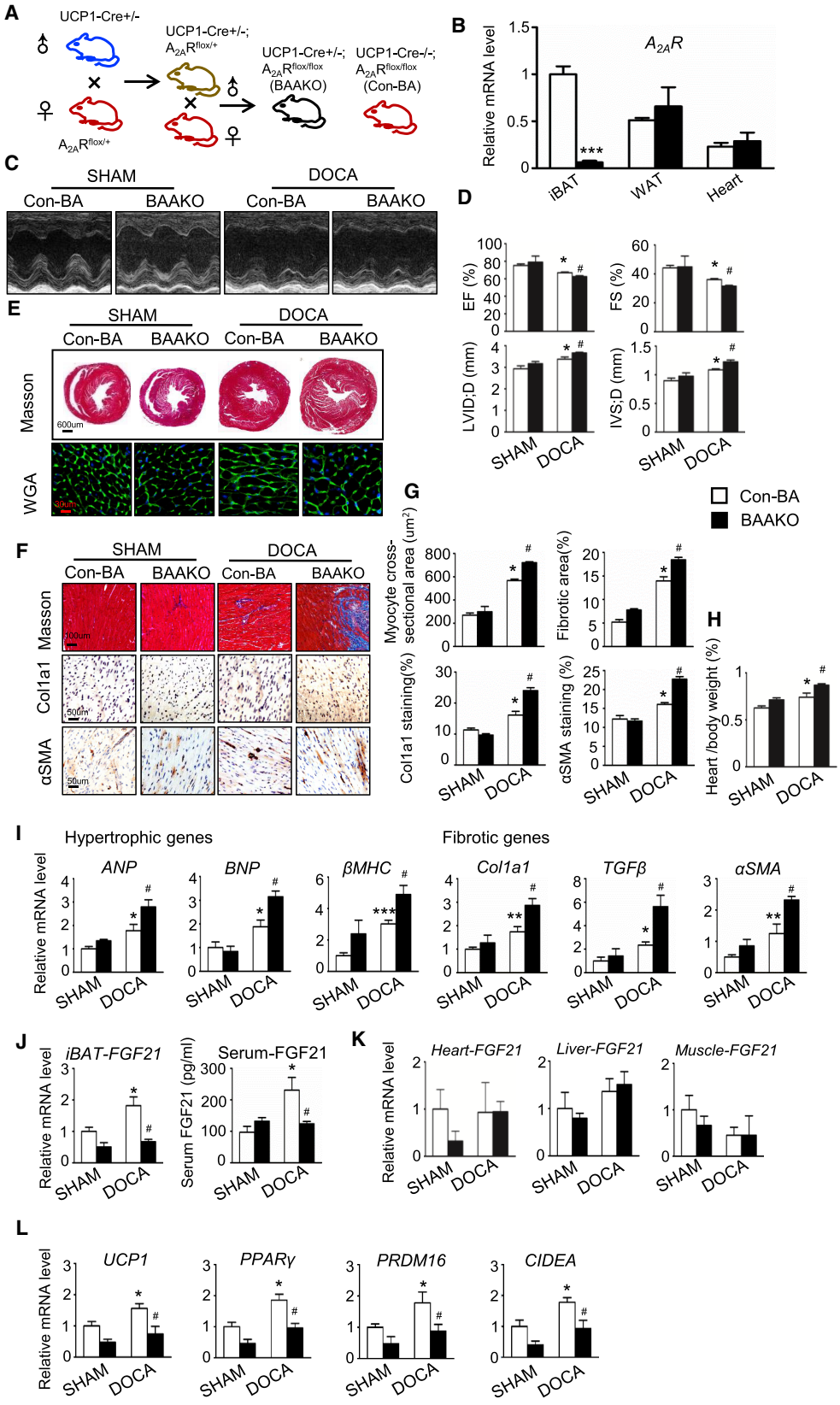

(legend on next page)

inhibited expression of thermogenic genes (*UCP1*, *PPARγ*, *PRDM16*, and *CIDEA*) in iBAT (Figure 6L). These results suggest that A_{2A}R-mediated brown adipocyte activation and FGF21 production is necessary for protecting against hypertensive cardiac remodeling.

A_{2A}R/FGF21 Pathway in Brown Adipocytes Protects against Hypertensive Cardiac Remodeling

To further understand the role of the BAT-derived A_{2A}R/FGF21 pathway in hypertensive cardiac remodeling, we generated brown adipocyte-specific FGF21KO (BAFKO) mice. $FGF21^{flox/+}$ mice were bred with UCP1-Cre mice, the UCP1-Cre+; $FGF21^{flox/flox}$ (BAFKO) and littermates UCP1-Cre-;$FGF21^{flox/flox}$ (Con-F) mice were treated with A_{2A}R agonist CGS21680 (1 mg/kg/day) or PBS, and these mice were then treated with DOCA-salt (Figure S7A). BAFKO blocked FGF21 expression in iBAT and reduced serum FGF21 level (Figures 7A and S7B), whereas local FGF21 mRNA expression in heart, liver, and muscle remained unchanged (Figure 7B). CGS21680 increased iBAT activity including smaller-sized adipocytes, increased UCP1 staining, and upregulation of thermogenic gene mRNA levels in Con-F hypertensive mice. However, these effects were absent in BAFKO hypertensive mice, suggesting an autocrine role of FGF21 on brown adipocyte activation (Figures S7C–S7E). More importantly, CGS21680 protected against hypertensive cardiac remodeling, including improved echocardiogram dysfunction, decreased left ventricular hypertrophy, and attenuated interstitial fibrosis after DOCA-salt treatment. However, these protective effects of CGS21680 were nullified in BAFKO mice (Figures 7C–7I). We herein provide direct evidence to support that brown adipocyte-derived FGF21 is required for A_{2A}R activation-mediated improvement of hypertensive cardiac remodeling.

DISCUSSION

In this study, we report that A_{2A}RKO attenuates BAT thermogenic activity and accelerates cardiac remodeling in DOCA-salt-induced hypertension. We demonstrated that A_{2A}R-mediated FGF21 production in BAT is critical for its cardiac protection. The effect of iBAT depletion-induced cardiac damage in hypertensive mice is blunted in A_{2A}RKO mice. Recombinant FGF21 administration improves cardiac remodeling in iBAT-depleted WT hypertensive mice. BAAKO but not CFAKO mice show accelerated hypertensive cardiac damage. Brown adipocyte-specific FGF21KO blocks the effects of A_{2A}R agonism in attenuating hypertensive cardiac remodeling. Taken together, the present study provides the first line of evidence for a direct crosstalk between BAT activity and cardiac protection in hypertension, which is largely dependent upon BAT A_{2A}R-mediated production of FGF21 and the endocrine function of FGF21 in the heart.

One of the major findings of the present study is the revelation of a novel role of iBAT in A_{2A}R-mediated inhibition of hypertensive cardiac remodeling. A_{2A}R is abundantly expressed in brain, heart, immune cells, and adipocytes (van Waarde et al., 2018). A_{2A}R activation can relax coronary arteries (Belardinelli et al., 1998). However, A_{2A}R appears to have limited direct effects on cardiac fibroblasts because of its low expression level and no effect on fibroblast extracellular matrix production (Dubey et al., 1998). Similarly, we observed that A_{2A}R agonist does not improve aldosterone-induced cardiac myocyte and fibroblast dysfunction. CFAKO does not affect DOCA-salt-induced hypertensive cardiac remodeling. On the other hand, A_{2A}R is highly expressed in adipose tissue, especially much more in iBAT than other tissues. Hypertension induces A_{2A}R upregulation in iBAT, but not in heart. A_{2A}R agonist-treated BAT adipocyte-conditioned medium attenuates aldosterone-induced cardiac fibroblast dysfunction and cardiomyocyte hypertrophy. Most importantly, BAAKO accelerates hypertensive cardiac remodeling. Consistently, surgical depletion of iBAT in WT mice augmented cardiac damage, whereas this operation has no effects on heart in A_{2A}RKO mice. Of course, it is worthy to note that we cannot completely exclude the contribution from cardiac A_{2A}R or other related tissues. A_{2A}R is also expressed in cardiomyocytes, which is important for myocyte survival (Hamad et al., 2010). Taken together, these findings clearly provide direct evidence supporting a significant contribution of A_{2A}R activation in brown adipocytes against hypertensive cardiac remodeling.

The second major finding of this study is to identify the BAT-derived bioactive substance FGF21 as the critical mediator of the protective effect of A_{2A}R activation in BAT against cardiac remodeling. Although adipose tissue-derived adipokines are known to play roles in the regulation of cardiovascular function, these typical adipokines are poorly expressed in BAT (Molica et al., 2015; Villarroya et al., 2017). Recently, BAT-derived batokines, which act in a paracrine or autocrine manner in adipocytes, have been identified (Villarroya et al., 2017). FGF21 is one of the first identified batokines, which promotes glucose utilization, improves glycemia and lipidemia, and induces adipocyte

Figure 6. Brown Adipocyte-Specific A_{2A}RKO Accelerates Cardiac Remodeling in Hypertensive Mice

(A) Illustration of hybridization protocol for brown adipocyte-specific A_{2A}RKO (BAAKO) mice and control Con-BA mice.
(B) qPCR analysis of mRNA expression level of A_{2A}R in iBAT, WAT, heart, liver, and muscle of BAAKO and Con-BA mice.
(C) Representative echocardiography images of Con-BA or BAAKO mice after SHAM or DOCA-salt treatment for 2 weeks.
(D) Quantitative analysis of EF, FS, LVID; D, and IVS; D obtained from echocardiography.
(E) Representative cross-sections of heart stained for Masson and WGA in CON-BA or BAAKO mice of SHAM or DOCA-salt mice.
(F) Representative cross-sections of heart stained for Masson, Col1a1, and αSMA in Con-BA or BAAKO mice after SHAM or DOCA-salt treatment for 2 weeks.
(G) Quantitative analysis of cardiomyocyte size (WGA staining), fibrotic area (blue area in Masson staining), Col1a1, and αSMA signals.
(H) The ratios of heart weight to body weight in Con-BA or BAAKO mice after SHAM or DOCA-salt treatment for 2 weeks.
(I) qPCR analysis of mRNA expression levels of hypertrophic and fibrotic genes in the heart.
(J) FGF21 expression level in iBAT and serum FGF21 concentration in Con-BA or BAAKO mice after SHAM or DOCA-salt treatment for 2 weeks.
(K) FGF21 expression level in heart, liver, and muscle of BAAKO and CON-BA mice after SHAM or DOCA-salt treatment for 2 weeks.
(L) qPCR analysis of mRNA expression levels of thermogenic genes in in Con-BA or BAAKO mice after SHAM or DOCA-salt treatment for 2 weeks.
Data are presented as means ± SEM; n = 6–9/group; $^{*}p < 0.05$, $^{**}p < 0.01$, $^{***}p < 0.001$ versus SHAM Con-BA mice, $^{\#}p < 0.05$ versus DOCA Con-BA mice.

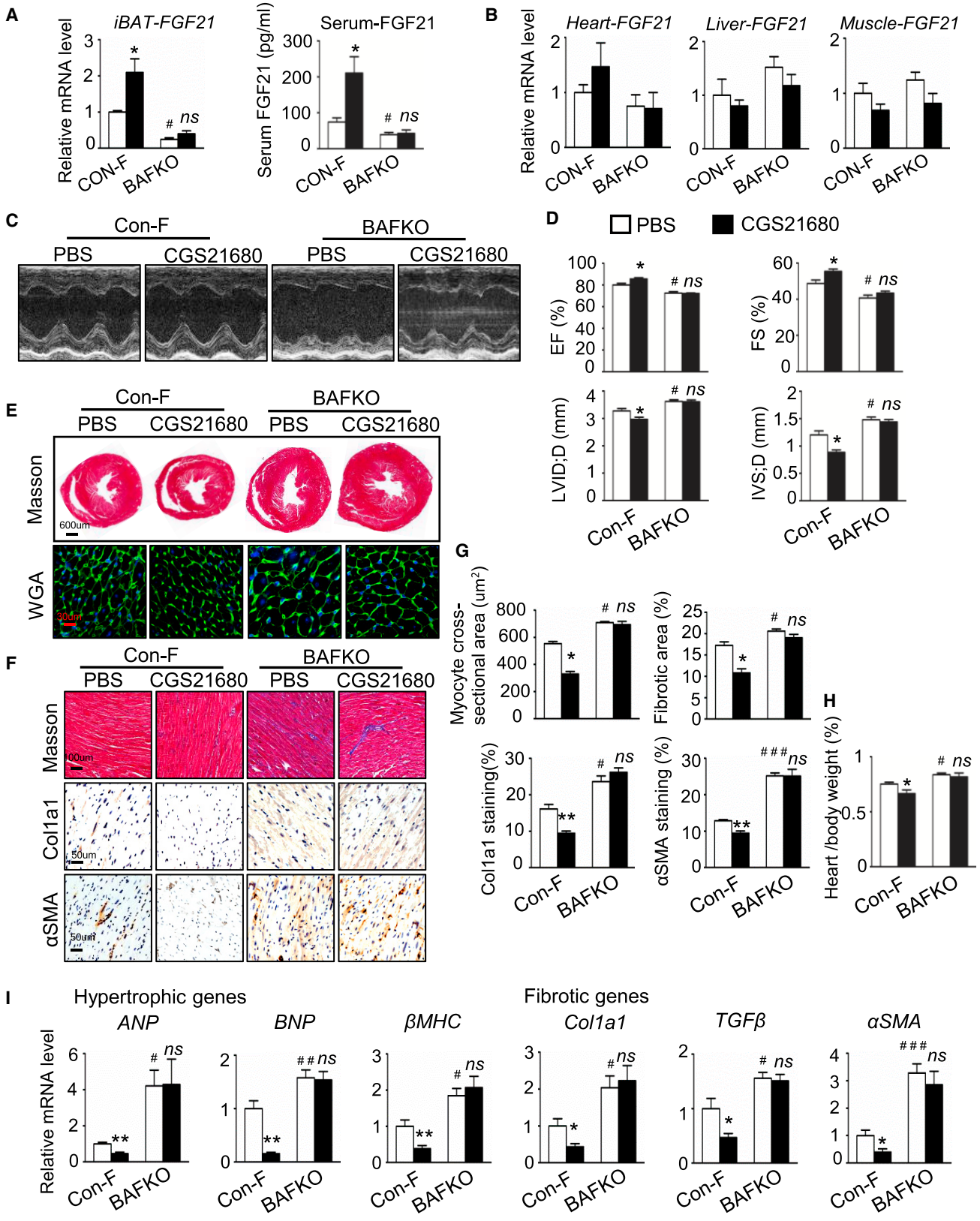

Figure 7. Brown Adipocyte-Specific FGF21KO Blocks the Effects of $A_{2A}R$ Agonism in Attenuating Hypertensive Cardiac Remodeling

(A) FGF21 expression level in iBAT and serum FGF21 concentration in Con-F and BAFKO DOCA-salt mice after PBS or CGS21680 treatment for 2 weeks.

(legend continued on next page)

browning (Douris et al., 2015; Fisher et al., 2012; Hondares et al., 2011). Cold-induced thermogenic activation or pharmacological-activated BAT could promote FGF21 production in the brown adipocytes (Lee et al., 2013; Quesada-Lopez et al., 2016). Herein we showed for the first time that A_{2A}R-mediated thermogenic activation promotes FGF21 production in BAT, which is capable of regulating circulation FGF21 level without affecting hepatic and cardiac FGF21 gene expression in hypertensive mice. Mechanistically, A_{2A}R-mediated AMPK signaling promotes transcription factor PGC1α expression, which is shown to induce FGF21 expression. Pharmacological antagonist of AMPK or knockdown of PGC1α represses A_{2A}R-mediated FGF21 expression in brown adipocytes. Heart is the key target as well as the source of FGF21, which is involved in inducing beneficial effects in cardiac remodeling (Planavila et al., 2013). However, little attention is given to the cardiac effects of FGF21 derived from other tissues. We demonstrate that BAT-derived FGF21 upon A_{2A}R activation plays an important endocrine role in hypertensive cardiac remodeling. Recombinant FGF21 administration improves iBAT depletion-induced dramatic cardiac remodeling in hypertensive mice. More importantly, brown adipocyte-specific FGF21KO blocks the effects of A_{2A}R agonism in attenuating hypertensive cardiac remodeling. These studies provide direct evidence that A_{2A}R-mediated FGF21 production in BAT plays a pivotal endocrine role in improving hypertensive cardiac remodeling.

Besides the effects on the metabolic process, FGF21 also participates in functional regulation of other tissues and organs. For example, FGF21 protects against immune senescence, and extends lifespan (Youm et al., 2016; Zhang et al., 2012). It also could regulate skeletal muscle homeostasis (Tezze et al., 2017). In the cardiovascular system, FGF21-mediated adiponectin production inhibits high fat diet-induced atherosclerosis (Lin et al., 2015). Therefore, our findings of A_{2A}R-mediated regulation of batokine FGF21 in BAT may represent an important endocrine role, not only in metabolic complications, but also in hypertensive cardiac remodeling. Notwithstanding the much more advanced complexity of human hypertensive cardiac injury in comparison with the mouse model, our novel findings suggest an attractive possibility that activation of BAT through A_{2A}R might serve as a potential therapeutic tool for prevention of hypertension-related cardiac damage.

Limitations of the Study

We show here that A_{2A}R-mediated FGF21 production in BAT is critical for improvement of hypertensive cardiac remodeling. Despite the novel and significant findings, there are several limitations in the present study. First, liver appears to be the main site for FGF21 production under physiological conditions, and further investigations need to assess the impact of the liver-derived FGF21 in hypertension. Second, although our data provide significant evidence that the A_{2A}R/FGF21pathway in BAT protects against hypertensive cardiac remodeling, whether this axis is involved in other hypertension-related target organ damage (e.g., vascular injury and renal fibrosis) is still unclear, and this needs to be explored in future study.

STAR★METHODS

Detailed methods are provided in the online version of this paper and include the following:

- KEY RESOURCES TABLE
- CONTACT FOR REAGENT AND RESOURCE SHARING
- EXPERIMENTAL MODEL AND SUBJECT DETAILS
  - Mice
  - DOCA-Salt-Induced Hypertension
  - IBAT Surgical Depletion
  - Cell Culture
- METHOD DETAILS
  - Echocardiography
  - *In Vivo* iBAT Imaging
  - Histological Analysis
  - QPCR Analysis
  - Western Blot Analysis
  - Co-Immunoprecipitation
  - FGF21 Measurements
  - Recombinant Lentiviruses
  - Cell Migration and Proliferation Assay
- QUANTIFICATION AND STATISTICAL ANALYSIS

SUPPLEMENTAL INFORMATION

Supplemental Information includes seven figures and one table and can be found with this article online at https://doi.org/10.1016/j.cmet.2018.06.013.

ACKNOWLEDGMENTS

We thank Professor Yu Huang (Institute of Vascular Medicine, Chinese University of Hong Kong) and Professor Y. Eugene Chen (Department of Internal Medicine, University of Michigan Medical Center) for valuable suggestions and critical reading of the manuscript. This work was supported by grants from the National Natural Science Foundation of China (91539202, 91739303, 81570221, and 81770495) and Shanghai Municipal Commission of Health and Family Planning (2017YQ076 and 201540222).

(B) FGF21 expression level in heart, liver, and muscle of Con-F and BAFKO DOCA-salt mice after PBS or CGS21680 treatment for 2 weeks.
(C) Representative echocardiography images of Con-F and BAFKO DOCA-salt mice after PBS or CGS21680 treatment for 2 weeks.
(D) Quantitative analysis of EF, FS, LVID; D, and IVS; D obtained from echocardiography.
(E) Representative cross-sections of heart stained for Masson and WGA in Con-F and BAFKO DOCA-salt mice after PBS or CGS21680 treatment for 2 weeks.
(F) Representative cross-sections of heart stained for Masson, Col1a1, and αSMA in Con-F and BAFKO DOCA-salt mice after PBS or CGS21680 treatment for 2 weeks.
(G) Quantitative analysis of cardiomyocyte size (WGA staining), fibrotic area (blue area in Masson staining), Col1a1, and αSMA signals.
(H) The ratio of heart weight to body weight ratios in Con-F and BAFKO DOCA-salt mice after PBS or CGS21680 treatment for 2 weeks.
(I) qPCR analysis of mRNA expression levels of hypertrophic and fibrotic genes in the heart (n = 5–7).
Data are presented as means ± SEM; n = 5–7/group; *$p < 0.05$, **$p < 0.01$, ***$p < 0.001$ versus PBS-treated Con-F DOCA mice, $^{\#}p < 0.05$, $^{\#\#}p < 0.01$, $^{\#\#\#}p < 0.001$ versus PBS-treated Con-F DOCA mice, ns indicates no statistical difference versus PBS treated BAFKO DOCA mice.

AUTHOR CONTRIBUTIONS

P.-J.G., C.-C.R., and L.-R.K. designed the experiments and wrote the paper. L.-R.K. and C.-C.R. performed the animal experiments and analytical methods. L.-R.K., X.-H.C., and X.-X.P. performed the *in vivo* images. L.-R.K., Y.M., and Z.-B.Z. performed *in vitro* work on adipocytes, cardiac myocytes, and fibroblasts. C.-C.R. and P.-J.G analyzed the data.

DECLARATION OF INTERESTS

The authors declare no competing interests.

Received: August 2, 2017
Revised: April 20, 2018
Accepted: June 15, 2018
Published: July 12, 2018

REFERENCES

Alonge, K.M., Meares, G.P., and Hillgartner, F.B. (2017). Glucagon and insulin cooperatively stimulate fibroblast growth factor 21 gene transcription by increasing the expression of activating transcription factor 4. J. Biol. Chem. *292*, 5239–5252.

Bahler, L., Molenaars, R.J., Verberne, H.J., and Holleman, F. (2015). Role of the autonomic nervous system in activation of human brown adipose tissue: a review of the literature. Diabetes Metab. *41*, 437–445.

Bastia, E., Xu, Y.H., Scibelli, A.C., Day, Y.J., Linden, J., Chen, J.F., and Schwarzschild, M.A. (2005). A crucial role for forebrain adenosine A(2A) receptors in amphetamine sensitization. Neuropsychopharmacology *30*, 891–900.

Belardinelli, L., Shryock, J.C., Snowdy, S., Zhang, Y., Monopoli, A., Lozza, G., Ongini, E., Olsson, R.A., and Dennis, D.M. (1998). The A2A adenosine receptor mediates coronary vasodilation. J. Pharmacol. Exp. Ther. *284*, 1066–1073.

Berk, B.C., Fujiwara, K., and Lehoux, S. (2007). ECM remodeling in hypertensive heart disease. J. Clin. Invest. *117*, 568–575.

Borea, P.A., Gessi, S., Merighi, S., and Varani, K. (2016). Adenosine as a multi-signalling guardian angel in human diseases: when, where and how does it exert its protective effects? Trends Pharmacol. Sci. *37*, 419–434.

Chau, M.D., Gao, J., Yang, Q., Wu, Z., and Gromada, J. (2010). Fibroblast growth factor 21 regulates energy metabolism by activating the AMPK-SIRT1-PGC-1alpha pathway. Proc. Natl. Acad. Sci. USA *107*, 12553–12558.

Chen, J.F., Huang, Z., Ma, J., Zhu, J., Moratalla, R., Standaert, D., Moskowitz, M.A., Fink, J.S., and Schwarzschild, M.A. (1999). A(2A) adenosine receptor deficiency attenuates brain injury induced by transient focal ischemia in mice. J. Neurosci. *19*, 9192–9200.

Chen, M.Z., Chang, J.C., Zavala-Solorio, J., Kates, L., Thai, M., Ogasawara, A., Bai, X., Flanagan, S., Nunez, V., Phamluong, K., et al. (2017). FGF21 mimetic antibody stimulates UCP1-independent brown fat thermogenesis via FGFR1/betaKlotho complex in non-adipocytes. Mol. Metab. *6*, 1454–1467.

Cittadini, A., Mantzoros, C.S., Hampton, T.G., Travers, K.E., Katz, S.E., Morgan, J.P., Flier, J.S., and Douglas, P.S. (1999). Cardiovascular abnormalities in transgenic mice with reduced brown fat: an animal model of human obesity. Circulation *100*, 2177–2183.

Coskun, T., Bina, H.A., Schneider, M.A., Dunbar, J.D., Hu, C.C., Chen, Y., Moller, D.E., and Kharitonenkov, A. (2008). Fibroblast growth factor 21 corrects obesity in mice. Endocrinology *149*, 6018–6027.

da Silva, J.S., Gabriel-Costa, D., Sudo, R.T., Wang, H., Groban, L., Ferraz, E.B., Nascimento, J.H., Fraga, C.A., Barreiro, E.J., and Zapata-Sudo, G. (2017). Adenosine A2A receptor agonist prevents cardiac remodeling and dysfunction in spontaneously hypertensive male rats after myocardial infarction. Drug Des. Devel. Ther. *11*, 553–562.

Douris, N., Stevanovic, D.M., Fisher, F.M., Cisu, T.I., Chee, M.J., Nguyen, N.L., Zarebidaki, E., Adams, A.C., Kharitonenkov, A., Flier, J.S., et al. (2015). Central fibroblast growth factor 21 browns white fat via sympathetic action in male mice. Endocrinology *156*, 2470–2481.

Drazner, M.H. (2011). The progression of hypertensive heart disease. Circulation *123*, 327–334.

Dubey, R.K., Gillespie, D.G., and Jackson, E.K. (1998). Adenosine inhibits collagen and protein synthesis in cardiac fibroblasts: role of A2B receptors. Hypertension *31*, 943–948.

Esler, M. (2015). The sympathetic nervous system in hypertension: back to the future? Curr. Hypertens. Rep. *17*, 11.

Fisher, F.M., Kleiner, S., Douris, N., Fox, E.C., Mepani, R.J., Verdeguer, F., Wu, J., Kharitonenkov, A., Flier, J.S., Maratos-Flier, E., et al. (2012). FGF21 regulates PGC-1alpha and browning of white adipose tissues in adaptive thermogenesis. Genes Dev. *26*, 271–281.

Gaich, G., Chien, J.Y., Fu, H., Glass, L.C., Deeg, M.A., Holland, W.L., Kharitonenkov, A., Bumol, T., Schilske, H.K., and Moller, D.E. (2013). The effects of LY2405319, an FGF21 analog, in obese human subjects with type 2 diabetes. Cell Metab. *18*, 333–340.

Gnad, T., Scheibler, S., von Kugelgen, I., Scheele, C., Kilic, A., Glode, A., Hoffmann, L.S., Reverte-Salisa, L., Horn, P., Mutlu, S., et al. (2014). Adenosine activates brown adipose tissue and recruits beige adipocytes via A2A receptors. Nature *516*, 395–399.

Hamad, E.A., Li, X., Song, J., Zhang, X.Q., Myers, V., Funakoshi, H., Zhang, J., Wang, J., Li, J., Swope, D., et al. (2010). Effects of cardiac-restricted overexpression of the A(2A) adenosine receptor on adriamycin-induced cardiotoxicity. Am. J. Physiol. Heart Circ. Physiol. *298*, H1738–H1747.

Hankir, M.K., Cowley, M.A., and Fenske, W.K. (2016). A BAT-centric approach to the treatment of diabetes: turn on the brain. Cell Metab. *24*, 31–40.

Holland, W.L., Adams, A.C., Brozinick, J.T., Bui, H.H., Miyauchi, Y., Kusminski, C.M., Bauer, S.M., Wade, M., Singhal, E., Cheng, C.C., et al. (2013). An FGF21-adiponectin-ceramide axis controls energy expenditure and insulin action in mice. Cell Metab. *17*, 790–797.

Holtwick, R., Gotthardt, M., Skryabin, B., Steinmetz, M., Potthast, R., Zetsche, B., Hammer, R.E., Herz, J., and Kuhn, M. (2002). Smooth muscle-selective deletion of guanylyl cyclase-A prevents the acute but not chronic effects of ANP on blood pressure. Proc. Natl. Acad. Sci. USA *99*, 7142–7147.

Hondares, E., Iglesias, R., Giralt, A., Gonzalez, F.J., Giralt, M., Mampel, T., and Villarroya, F. (2011). Thermogenic activation induces FGF21 expression and release in brown adipose tissue. J. Biol. Chem. *286*, 12983–12990.

Jeanson, Y., Ribas, F., Galinier, A., Arnaud, E., Ducos, M., Andre, M., Chenouard, V., Villarroya, F., Casteilla, L., and Carriere, A. (2016). Lactate induces FGF21 expression in adipocytes through a p38-MAPK pathway. Biochem. J. *473*, 685–692.

Kliewer, S.A., and Mangelsdorf, D.J. (2010). Fibroblast growth factor 21: from pharmacology to physiology. Am. J. Clin. Nutr. *91*, 254S–257S.

Kozak, L.P. (2010). Brown fat and the myth of diet-induced thermogenesis. Cell Metab. *11*, 263–267.

Lau, W.B., Ohashi, K., Wang, Y., Ogawa, H., Murohara, T., Ma, X.L., and Ouchi, N. (2017). Role of adipokines in cardiovascular disease. Circ. J. *81*, 920–928.

Ledent, C., Vaugeois, J.M., Schiffmann, S.N., Pedrazzini, T., El Yacoubi, M., Vanderhaeghen, J.J., Costentin, J., Heath, J.K., Vassart, G., and Parmentier, M. (1997). Aggressiveness, hypoalgesia and high blood pressure in mice lacking the adenosine A2a receptor. Nature *388*, 674–678.

Lee, P., Brychta, R.J., Linderman, J., Smith, S., Chen, K.Y., and Celi, F.S. (2013). Mild cold exposure modulates fibroblast growth factor 21 (FGF21) diurnal rhythm in humans: relationship between FGF21 levels, lipolysis, and cold-induced thermogenesis. J. Clin. Endocrinol. Metab. *98*, E98–E102.

Lee, P., Linderman, J.D., Smith, S., Brychta, R.J., Wang, J., Idelson, C., Perron, R.M., Werner, C.D., Phan, G.Q., Kammula, U.S., et al. (2014). Irisin and FGF21 are cold-induced endocrine activators of brown fat function in humans. Cell Metab. *19*, 302–309.

Lin, Z., Pan, X., Wu, F., Ye, D., Zhang, Y., Wang, Y., Jin, L., Lian, Q., Huang, Y., Ding, H., et al. (2015). Fibroblast growth factor 21 prevents atherosclerosis by suppression of hepatic sterol regulatory element-binding protein-2 and induction of adiponectin in mice. Circulation *131*, 1861–1871.

Liu, X., Xiao, J., Zhu, H., Wei, X., Platt, C., Damilano, F., Xiao, C., Bezzerides, V., Bostrom, P., Che, L., et al. (2015). miR-222 is necessary for exercise-induced cardiac growth and protects against pathological cardiac remodeling. Cell Metab. *21*, 584–595.

Lowell, B.B., S-Susulic, V., Hamann, A., Lawitts, J.A., Himms-Hagen, J., Boyer, B.B., Kozak, L.P., and Flier, J.S. (1993). Development of obesity in transgenic mice after genetic ablation of brown adipose tissue. Nature *366*, 740–742.

MacDougald, O.A., Hwang, C.S., Fan, H., and Lane, M.D. (1995). Regulated expression of the obese gene product (leptin) in white adipose tissue and 3T3-L1 adipocytes. Proc. Natl. Acad. Sci. USA *92*, 9034–9037.

Markan, K.R., Naber, M.C., Ameka, M.K., Anderegg, M.D., Mangelsdorf, D.J., Kliewer, S.A., Mohammadi, M., and Potthoff, M.J. (2014). Circulating FGF21 is liver derived and enhances glucose uptake during refeeding and overfeeding. Diabetes *63*, 4057–4063.

Mattu, H.S., and Randeva, H.S. (2013). Role of adipokines in cardiovascular disease. J. Endocrinol. *216*, T17–T36.

Mechanick, J.I., Zhao, S., and Garvey, W.T. (2016). The adipokine-cardiovascular-lifestyle network: translation to clinical practice. J. Am. Coll. Cardiol. *68*, 1785–1803.

Molica, F., Morel, S., Kwak, B.R., Rohner-Jeanrenaud, F., and Steffens, S. (2015). Adipokines at the crossroad between obesity and cardiovascular disease. Thromb. Haemost. *113*, 553–566.

Peleli, M., and Carlstrom, M. (2017). Adenosine signaling in diabetes mellitus and associated cardiovascular and renal complications. Mol. Aspects Med. *55*, 62–74.

Planavila, A., Redondo-Angulo, I., Ribas, F., Garrabou, G., Casademont, J., Giralt, M., and Villarroya, F. (2015). Fibroblast growth factor 21 protects the heart from oxidative stress. Cardiovasc. Res. *106*, 19–31.

Planavila, A., Redondo, I., Hondares, E., Vinciguerra, M., Munts, C., Iglesias, R., Gabrielli, L.A., Sitges, M., Giralt, M., van Bilsen, M., et al. (2013). Fibroblast growth factor 21 protects against cardiac hypertrophy in mice. Nat. Commun. *4*, 2019.

Potthoff, M.J., Inagaki, T., Satapati, S., Ding, X., He, T., Goetz, R., Mohammadi, M., Finck, B.N., Mangelsdorf, D.J., Kliewer, S.A., et al. (2009). FGF21 induces PGC-1alpha and regulates carbohydrate and fatty acid metabolism during the adaptive starvation response. Proc. Natl. Acad. Sci. USA *106*, 10853–10858.

Quesada-Lopez, T., Cereijo, R., Turatsinze, J.V., Planavila, A., Cairo, M., Gavalda-Navarro, A., Peyrou, M., Moure, R., Iglesias, R., Giralt, M., et al. (2016). The lipid sensor GPR120 promotes brown fat activation and FGF21 release from adipocytes. Nat. Commun. *7*, 13479.

Rice, D.R., White, A.G., Leevy, W.M., and Smith, B.D. (2015). Fluorescence imaging of interscapular brown adipose tissue in living mice. J. Mater. Chem. B *3*, 1979–1989.

Ruan, C.C., Ge, Q., Li, Y., Li, X.D., Chen, D.R., Ji, K.D., Wu, Y.J., Sheng, L.J., Yan, C., Zhu, D.L., et al. (2015). Complement-mediated macrophage polarization in perivascular adipose tissue contributes to vascular injury in deoxycorticosterone acetate-salt mice. Arterioscler. Thromb. Vasc. Biol. *35*, 598–606.

Sambeat, A., Gulyaeva, O., Dempersmier, J., Tharp, K.M., Stahl, A., Paul, S.M., and Sul, H.S. (2016). LSD1 interacts with Zfp516 to promote UCP1 transcription and brown fat program. Cell Rep. *15*, 2536–2549.

Sidossis, L., and Kajimura, S. (2015). Brown and beige fat in humans: thermogenic adipocytes that control energy and glucose homeostasis. J. Clin. Invest. *125*, 478–486.

Tezze, C., Romanello, V., Desbats, M.A., Fadini, G.P., Albiero, M., Favaro, G., Ciciliot, S., Soriano, M.E., Morbidoni, V., Cerqua, C., et al. (2017). Age-associated loss of OPA1 in muscle impacts muscle mass, metabolic homeostasis, systemic inflammation, and epithelial senescence. Cell Metab. *25*, 1374–1389.e6.

Thoonen, R., Ernande, L., Cheng, J., Nagasaka, Y., Yao, V., Miranda-Bezerra, A., Chen, C., Chao, W., Panagia, M., Sosnovik, D.E., et al. (2015). Functional brown adipose tissue limits cardiomyocyte injury and adverse remodeling in catecholamine-induced cardiomyopathy. J. Mol. Cell. Cardiol. *84*, 202–211.

van Waarde, A., Dierckx, R., Zhou, X., Khanapur, S., Tsukada, H., Ishiwata, K., Luurtsema, G., de Vries, E.F.J., and Elsinga, P.H. (2018). Potential therapeutic applications of adenosine A2A receptor ligands and opportunities for A2A receptor imaging. Med. Res. Rev. *38*, 5–56.

Villarroya, F., Cereijo, R., Villarroya, J., and Giralt, M. (2017). Brown adipose tissue as a secretory organ. Nat. Rev. Endocrinol. *13*, 26–35.

Yaqoob, U., Jagavelu, K., Shergill, U., de Assuncao, T., Cao, S., and Shah, V.H. (2014). FGF21 promotes endothelial cell angiogenesis through a dynamin-2 and Rab5 dependent pathway. PLoS One *9*, e98130.

Youm, Y.H., Horvath, T.L., Mangelsdorf, D.J., Kliewer, S.A., and Dixit, V.D. (2016). Prolongevity hormone FGF21 protects against immune senescence by delaying age-related thymic involution. Proc. Natl. Acad. Sci. USA *113*, 1026–1031.

Zhang, C., Huang, Z., Gu, J., Yan, X., Lu, X., Zhou, S., Wang, S., Shao, M., Zhang, F., Cheng, P., et al. (2015). Fibroblast growth factor 21 protects the heart from apoptosis in a diabetic mouse model via extracellular signal-regulated kinase 1/2-dependent signalling pathway. Diabetologia *58*, 1937–1948.

Zhang, Y., Xie, Y., Berglund, E.D., Coate, K.C., He, T.T., Katafuchi, T., Xiao, G., Potthoff, M.J., Wei, W., Wan, Y., et al. (2012). The starvation hormone, fibroblast growth factor-21, extends lifespan in mice. eLife *1*, e00065.

Please cite this article in press as: Ruan et al., A_{2A} Receptor Activation Attenuates Hypertensive Cardiac Remodeling via Promoting Brown Adipose Tissue-Derived FGF21, Cell Metabolism (2018), https://doi.org/10.1016/j.cmet.2018.06.013

STAR★METHODS

KEY RESOURCES TABLE

REAGENT or RESOURCE	SOURCE	IDENTIFIER
Antibodies		
Rabbit polyclonalAnti-Col1a1	Santa Cruz	Cat#sc-8784; RRID:AB_638601
Rabbit polyclonal Anti-TGFβ	Cell Signaling Technology	Cat #3711S; RRID:AB_10695720
Mouse monoclonal Anti-αSMA	Sigma-Aldrich	Cat #A5228: RRID:AB_262054
Rabbit polyclonalAnti-UCP1	Abcam	Cat #ab23841; RRID:AB_2213764
Mouse monoclonal Anti-PPARγ	Santa Cruz	Cat #sc-7273; RRID:AB_628115
Rabbit polyclonalAnti-PRDM16	Abcam	Cat #ab106410; RRID:AB_10866455
Rabbit polyclonal Anti-CIDE A	Abcam	Cat #ab8402; RRID:AB_306536
Goat polyclonal Anti-Perrilipin	Abcam	Cat #ab61682;RRID:AB_944751
Rabbit monoclonalAnti-FGF21	Abcam	Cat #ab171941; RRID:AB_2629460
Mouse monoclonalAnti-A2AR	Santa Cruz	Cat #sc-32261; RRID:AB_2226517
Rabbit polyclonalAnti-PGC1α	Santa Cruz	Cat #sc-13067; RRID:AB_2166218
GAPDH monoclonal antibody	Proteintech	Cat #HRP-60004; RRID:AB_2107436
Rabbit monoclonal Anti-p-AMPKα	Cell Signaling Technology	Cat #2535S; RRID:AB_331250
Rabbit polyclonal Anti-AMPKα	Cell Signaling Technology	Cat #2532S; RRID:AB_330331
Rabbit polyclonal Anti-p-PKA	Cell Signaling Technology	Cat #5661; RRID:AB_10707163
Rabbit monoclonal Anti-PKA	Cell Signaling Technology	Cat #4782; RRID:AB_2170170
Rabbit monoclonal Anti-p-AKT	Cell Signaling Technology	Cat #4060; RRID:AB_2315049
Rabbit monoclonal Anti-AKT	Cell Signaling Technology	Cat #4691; RRID:AB_915783
Rabbit monoclonal Anti –p-P38 MAPK	Cell Signaling Technology	Cat #4511; RRID:AB_2139682
Rabbit monoclonal Anti –P38 MAPK	Cell Signaling Technology	Cat #9212; RRID:AB_330713
Goat polyclonal Anti-KLB	R&D Systems	Cat #AF2619
Rabbit Anti-FGF Receptor1	Cell Signaling Technology	Cat #9740; RRID:AB_2131932
Normal rabbit IgG	Santa Cruz	Cat #sc2027; RRID:AB_737197
Alexa 488 donkey anti-rabbit	Invitrogen	Cat #A21206; RRID:AB_2535792
Alexa 594 donkey anti-rabbit	Invitrogen	Cat #A21207; RRID:AB_141637
Alexa 594 donkey anti-goat	Invitrogen	Cat #A11055; RRID:AB_2534102
Bacterial and Virus Strains		
Lentiviral control siRNA	GeneChem	N/A
Lentiviral sh-PGC1α	GeneChem	N/A
Chemicals, Peptides, and Recombinant Proteins		
DOCA (50 mg, 21 Days)	Innovative Research of America	Cat #M-121
CGS21680	Selleck Chemicals	Cat #S2153
KW6002	Selleck Chemicals	Cat #S2790
rFGF21	Sino Biological Inc	Cat#10911-H07E
SRFluor680	MolecularTargeting Technologies	Cat #SR-1010
Collagenase, type II	Sigma-Aldrich	Cat #C6885
Insulin	Sigma-Aldrich	Cat #91077C
Triiodothyronine (T3)	Sigma-Aldrich	Cat #T2877
3-Isobutyl-1-methylxanthine (IBMX)	Sigma-Aldrich	Cat #I7018
Dexamethasone	Sigma-Aldrich	Cat #D4902
Rosiglitazone	Sigma-Aldrich	Cat #2408
5-bromodeoxyuridine	Sigma-Aldrich	Cat #5002
Aldosterone	Sigma-Aldrich	Cat #706035
Compound C	SelleckChemicals	Cat #866405-64-3

(*Continued on next page*)

Continued

REAGENT or RESOURCE	SOURCE	IDENTIFIER
RIPA lysis buffer	Millipore	Cat #20-188
Protease Inhibitor Cocktail	Biotool	Cat #B14002
Phosphatase Inhibitor Cocktail	Biotool	Cat #B15001
DAPI (4',6-Diamidino-2-Phenylindole, Dihydrochloride)	Invitrogen	Cat#D1306
Trizol Reagent	Invitrogen	Cat#15596-018
Protein A/G magnetic bead	Bimake	Cat #B23202
Critical Commercial Assays		
Mouse FGF-21 ELISA Kit	R&D	Cat #MF2100
Click-iT EdU Alexa Fluor 555 Imaging kit	Invitrogen	Cat #10639
BCA Protein Assay Kit	Beyotime	Cat #P0010
Transcription Master Mix	Promega	Cat # 07912323001
SYBR Green qPCR Master Mix	Takara	Cat #RR420B
Masson trichrome stain kit	Servicebio	Cat #G1006
Experimental Models: Cell Lines		
Primary adipocytes	Quesada-Lopez et al., 2016	N/A
Primary cardiac fibroblasts	Dubey et al., 1998	N/A
Primary cardiomyocytes	Liu et al., 2015	N/A
Experimental Models: Organisms/Strains		
C57BL/6J mice	The Jackson Laboratory	Cat #000664
BALB/c mice	The Jackson Laboratory	Cat #000651
A_{2A}RKO mice	The Jackson Laboratory	Cat #010685
$A_{2A}R^{flox}$ mice	The Jackson Laboratory	Cat #010678
$FGF21^{flox}$ mice	The Jackson Laboratory	Cat #022361
UCP1-Cre mice	The Jackson Laboratory	Cat #024670
SM22α-Cre mice	The Jackson Laboratory	Cat #017491
Oligonucleotides		
Primers for qPCR	See Table S1	N/A
Software and Algorithms		
ImagePro Plus 7	Media Cybernetics	http://www.mediacy.com/imageproplus
GraphPad Prism 7	Graph Pad	https://www.graphpad.com/
SPSS 23	IBM	https://www.ibm.com/products/spss-statistics
Other		
Cell Strainer, 40 μm Nylon	Falcon	Cat #352340
Transwell Chamber	Corning	Cat #3422

CONTACT FOR REAGENT AND RESOURCE SHARING

Further information and requests for resources and reagents should be directed to and will be fulfilled by the Lead Contact, Ping-Jin Gao (gaopingjin@sibs.ac.cn).

EXPERIMENTAL MODEL AND SUBJECT DETAILS

Mice

$A_{2A}R$ knockout (A_{2A}RKO) (BALB/c background) (Chen et al., 1999), $A_{2A}R^{flox}$ (C57BL/6J background) (Bastia et al., 2005), $FGF21^{flox}$ (C57BL/6J background) (Potthoff et al., 2009), UCP1-Cre (C57BL/6J background) (Sambeat et al., 2016) and SM22α-Cre (C57BL/6J background) (Holtwick et al., 2002) mice were all obtained from the Jackson Laboratory. $A2AR^{flox}$ mice were bred with UCP1-Cre mice to produce UCP1-Cre+;$A2AR^{flox}$ heterozygote mice. Then the heterozygote mice were bred with $A2AR^{flox/flox}$ mice to produce UCP1-Cre+;$A2AR^{flox/flox}$ (BAAKO) homozygote and littermates UCP1-Cre-;A2AR-flox/flox (Con-BA)= mice.

$A_{2A}R^{flox}$ mice were bred with SM22α-Cre mice to produce SM22α-Cre+;$A_{2A}R^{flox}$ heterozygote mice. Then the heterozygote mice were bred with A_{2A}R-flox/flox mice to produce SM22α-Cre+;$A_{2A}R^{flox/flox}$ (CFAKO) homozygote and littermates SM22α-Cre-; $A_{2A}R^{flox/flox}$ (Con-CF) mice.

$FGF21^{flox}$ mice were bred with UCP1-Cre mice to produce UCP1-Cre+;$FGF21^{flox}$ heterozygote mice. Then the heterozygote mice were bred with $FGF21^{flox/flox}$ mice to produce UCP1-Cre+;$FGF21^{flox/flox}$ (BAFKO) homozygote and littermates UCP1-Cre-; $FGF21^{flox/flox}$ (Con-F) mice. Male mice of 10-12 weeks old were in used in all experiments.

DOCA-Salt-Induced Hypertension

Mice were uninephrectomized and randomly assigned to sham group or DOCA-salt group that received a DOCA pellet (50 mg/pellet) subcutaneously together with 1% NaCl in the drinking water for 2 weeks (Ruan et al., 2015). For pharmacological investigation, DOCA-salt mice received intraperitoneally injection of A_{2A}Ragonist CGS21680 (1 mg/kg/day), another group received PBS only. All animal experiments were conducted in accordance with guidelines approved by the Institutional Guidelines established by the Committee of Ethics on Animal Experiments at Shanghai Jiao Tong University School of Medicine.

IBAT Surgical Depletion

Mice was exposed to euthanasia by 1.5% pentobarbital Sodium (85-100 mg/kg body weight) and the iBAT was surgically depleted as previously described (Thoonen et al., 2015). Mice that were sham operated underwent the same procedure, their iBAT pad was located, exposed, and then been closed. In some experiments, these mice were intraperitoneally injected with rFGF21 protein (0.3 mg/kg/day).

Cell Culture

Primary preadipocytes were isolated from iBAT as previously described (Quesada-Lopez et al., 2016). Cells were differentiated into adipocytes in 10% FBS DMEM/F12 culture medium supplemented with an adipogenic cocktail (0.5 mM IBMX, 1 mM dexamethasone,1 mM rosiglitazone, 0.02 mM insulin, and 1 nM T3) for 48 hr, then were maintained in 0.02 mM insulin and 1 nM T3 and harvested at day 6-8 post-differentiation.

Primary cardiac fibroblasts (CFs) were isolated from 3-4 weeks-old male mice as previously described (Dubey et al., 1998). Cells were cultured in DMEM supplemented with 15% FBS and 1% penicillin and streptomycin. Neonatal mouse cardiomyocytes (NMCMs) were isolated from 1-3 days-old BALB/c mouse as previously described (Liu et al., 2015). NMCMs were grown in DMEM supplemented with 15% FBS, 1% penicillin and streptomycin and 100 μM 5-bromodeoxyuridine for 48 hr. To induce hypertrophy, NMCMs were cultured in serum-free DMEM for 12 hr and treated with aldosterone for 2 hr. For other experiments, NMCMs were also treated with CGS21680 (150nM), KW6002 (100 nM) or rFGF21 (100 nM) at several time points.

METHOD DETAILS

Echocardiography

Transthoracic echocardiography was performed with a Vevo 2,100 instrument (Fuji Film Visual Sonics) equipped with an MS-400 imaging transducer (18-38 MHz) as previously described (Planavila et al., 2013). Briefly, mice were preconditioned by chest hair removal, anaesthetized with 1%-2% isoflurane administered via inhalation, and maintained in a supine position on a dedicated animal handling platform with limbs attached for electrocardiogram gating during imaging. Body temperature was kept constant by feeding the signal of a rectal probe back to a heating pad, while heart and respiratory rates were continuously monitored. M-mode recording was performed at the midventricular level. All images were analyzed using dedicated software (Vevo 2,100 version 1.4). LV wall thickness (LVID;D) and inter ventricular septum (IVS;D) at diastole were measured. Percent LV ejection fraction (EF) and fractional shortening (FS) was calculated from M-mode measurements. All procedures were performed under double-blind conditions with regard to genotype or treatment.

In Vivo iBAT Imaging

The iBAT imaging was performed as previously described (Rice et al., 2015). Briefly, mice were intravenously injected with micellar SRFluor680 (0.35 mg in 100 μL PBS), After 6-8 hr, mice were anesthetized with 1%-2% isoflurane with an oxygen flow rate of 2 L/min and denuded by depilatory cream to reduce scattering and absorption by the hair. Fluorescence imaging was obtained from IVIS Spectrum/CT system (PerkinElmer) following the manufacture introductions. The fluorescence acquisition parameters were: Excitation Filter: 615-665 nm, Excitation Filter: 695-770 nm, Acquisition time: 10 seconds, Subject height: 1.5 cm, Field of view: A (2 cm*2 cm). Then the CT imaging and 3D Reconstruction was obtained through X-Rays Acquire mode. Data analysis and the photon flux data were obtained by using Region of Interest (ROI) tools.

Histological Analysis

Heart and adipose tissues were fixed in 4% paraformaldehyde and embedded into paraffin, and then 5 μm sections were prepared for hematoxylin and eosin (HE), Masson's trichrome (masson) or wheat germ agglutinin (WGA) staining as previously described (Liu et al., 2015). Morphometric analysis was performed using Image-Pro Plus software to assess cardiac fibrosis by measuring

the percentage of stained area (blue) to the total area. For immunohistochemical staining, heart sections were incubated with primary antibodies for Col1a1 (1:100) or αSMA (1:1000). Adipose tissue sections were incubated with primary antibody for UCP1 (1:100). For immunofluorescence staining, adipose tissue was incubated with primary antibodies for PLIN (1:200) and p-AMPK (1:100), or PGC1α (1:100) and FGF21 (1:100).

QPCR Analysis

Total RNA was extracted from tissues and cultured cells using TRIzol (Invitrogen) followed by chloroform extraction according to the manufacturer's protocol. Aliquots of total RNA were reverse transcribed into single-stranded cDNA by incubation with moloney murine leukemia virus reverse transcriptase (Promega). Real-time qRT-PCR was performed with SYBR Premix Ex Taq kits with ROX (TaKaRa) according to manufacturer's instructions. Signals were detected on an ABI PRISM 7,900 machine (Applied Biosystems). GAPDH was used as a standard reference. Reactions were done at 95°C for 30 s followed by 40 cycles of 95°C for 5 s, 60°C for 30 s. Sequences of primers used in this study are provided in Table S1.

Western Blot Analysis

Western blot was performed as previously reported (Ruan et al., 2015). Briefly, frozen tissues were powdered and then homogenized in ice-cold RIPA buffer (50 mM Tris-HCl (pH 7.4); 10% Nonidet P-40; 0.25% sodium deoxycholate; 150 mM NaCl; 1 mM EDTA; 0.5 M NaF; 10 mM sodium pyrophosphate) supplemented with protease inhibitor cocktail (Biotool) and phosphatase inhibitor (Biotool). Cultured cells were directly lysed in RIPA buffer. Protein was run on a 12% SDS page gel and blotted onto PVDF membrane (Millipore) by wet transfer. The blots were first incubated with Col1a1 (1:1000), αSMA (1:4000), TGFβ (1:1000), A_{2A}R (1:1000), FGF21(1:1000), FGFR1 (1:1000), KLB (1:1000), PGC1α (1:1000), p-AMPK (1:1000), t-AMPK (1:4000), p-PKA (1:1000), t-PKA (1:4000), p-AKT (1:1000), t-AKT (1:4000), p-P38 MAPK (1:1000), t-P38 MAPK (1:4000) and GAPDH (1:4000) antibodies in blocking buffer containing PBS, 1% Milk, and 0.02% Tween 20. Secondary HPR conjugated antibody in blocking buffer was applied for 2 hr at room temperature. Following 3 washes in PBS containing 0.02% Tween 20 for 10 min per wash, the signal was detected by chemiluminescence.

Co-Immunoprecipitation

Recombinant FGF21 protein (6×His tag)-treated primary cardiac fibroblasts were washed in PBS. Cells were lysed in ice-cold IP Lysis/Wash Buffer (Thermo). Frozen heart tissues were powdered and then homogenized in ice-cold RIPA buffer supplemented with protease inhibitor cocktail (Biotool). Whole cell lysate was stored on ice for the following step. Transfer 50 μL protein A/G magnetic bead slurry to a 1.5 mL tube, then wash the slurry in binding buffer. Whole-cell lysates were mixed with mouse anti-6×His tag antibody (50 μg/mL) or normal mouse IgG for 1 hr at room temperature. Bead slurry (50 μL) was subsequently added and mixed with whole-cell lysates for 1 hr at room temperature. The beads were washed three times with lysis buffer. Samples were eluted into SDS Loading Buffer and analyzed by western blot.

FGF21 Measurements

Serum was obtained from blood collected from mice. Conditioned medium was obtained from cultured adipocytes. FGF21 levels in blood or conditioned medium were determined by using Mouse FGF21 ELISA-Kit (R&D) according to the manufacturer's instructions. Data are expressed in pg/mL.

Recombinant Lentiviruses

Mouse PGC1α shRNA and control scramble shRNA were constructed using pGCSIL-GFP (Addgene). PGC1α shRNA sequence: ACT ATT GAG CGA ACC TTA A, no-target control shRNA sequence: TTC TCC GAA CGT GTC ACG T. Lentiviruses carrying shRNA were produced and purified by GeneChem. The viruses were used to infect cells in the presence of Polybrene. Forty-eight hours later, primary cultured adipocytes were lysed with Trizol reagent or RIPA buffer, and the expression of PGC1α was confirmed by qPCR and western blot analysis.

Cell Migration and Proliferation Assay

Cardiac fibroblast migration was measured by transwell invasion assay. Briefly, the cells (5×10^4 cells per well) were cultured in the top chamber with serum-free DMEM medium, 800 μL complete media with 10% FBS was added into the lower chamber. CGS21680 or KW6002 was added into the lower chamber, respectively. After 24 hr of cultivation, nonvading cells was gently wiped with a cotton swab, and the invaded cells were fixed in 4% paraformaldehyde, stained with 1% crystal violet solution (Sigma), and counted in selected randomly five fields under a light microscope (Olympus, Tokyo, Japan).

We assayed proliferation using the Click-iT EdU Alexa Fluor 555 Imaging kit (Invitrogen). Briefly, we incubated live cells with EdU (20 μM) for 1 hr before fixation and stained nuclei according to the manufacturer's guidelines. We counterstained nuclei with DAPI (Invitrogen). Data analyses were blinded, where researchers performing cell scoring were unaware of the treatment condition given to the sample groups analyzed.

QUANTIFICATION AND STATISTICAL ANALYSIS

All data are expressed as means ± SEM. Statistical analysis was performed using one-tailed or two-tailed Student's t test. Normal distribution of the variables of interest was checked using the Student's t test. For experiments in which more than two groups should be compared, one-way ANOVA followed by the post hoc Dunnett's test for data with more than 2 groups (Levene's tests for equal variance). Dunnett's T3 test was used for post hoc test comparison for the analysis of unequal variances (Welch's and Brown-Forsythe's test). P value of 0.05 or less was deemed statistically significant in all of these statistical tests. Statistical details and results of experiments are found in the figures and figure legends.